JCI The Journal of Clinical Investigation

TNFR2/14-3-3ε signaling complex instructs macrophage plasticity in inflammation and autoimmunity

Wenyu Fu, … , Png Loke, Chuan-ju Liu

J Clin Invest. 2021;131(16):e144016. https://doi.org/10.1172/JCI144016.

Research Article | Autoimmunity | Inflammation

Graphical abstract

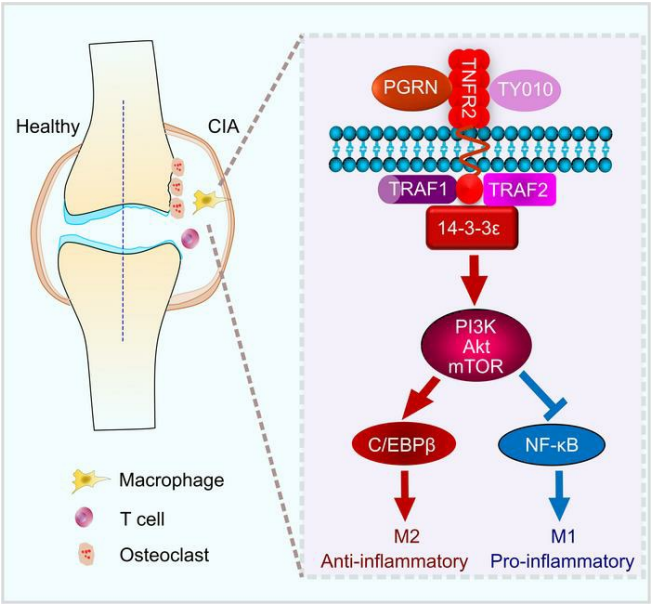

TNFR2/14-3-3ε signaling complex instructs macrophage plasticity in inflammation and autoimmunity

Wenyu Fu,[1] Wenhuo Hu,[2] Young-Su Yi,[1] Aubryanna Hettinghouse,[1] Guodong Sun,[1] Yufei Bi,[1] Wenjun He,[1] Lei Zhang,[1] Guanmin Gao,[1] Jody Liu,[1] Kazuhito Toyo-oka,[3] Guozhi Xiao,[4] David B. Solit,[2,5] Png Loke,[6] and Chuan-ju Liu[1,7]

[1]Department of Orthopedic Surgery, New York University Grossman School of Medicine, New York, New York, USA. [2]Human Oncology and Pathogenesis Program and Marie-Josée and Henry R. Kravis Center for Molecular Oncology, Memorial Sloan Kettering Cancer Center, New York, New York, USA. [3]Department of Neurobiology and Anatomy, Drexel University College of Medicine, Philadelphia, Pennsylvania, USA. [4]Department of Biochemistry, School of Medicine, Guangdong Provincial Key Laboratory of Cell Microenvironment and Disease Research, Shenzhen Key Laboratory of Cell Microenvironment, Southern University of Science and Technology, Shenzhen, China. [5]Genitourinary Oncology Service, Department of Medicine, Memorial Sloan Kettering Cancer Center, New York, New York, USA. [6]Department of Microbiology, New York University Grossman School of Medicine, New York, New York, USA. [7]Department of Cell Biology, New York University Grossman School of Medicine, New York, New York, USA.

TNFR1 and TNFR2 have received prominent attention because of their dominance in the pathogenesis of inflammation and autoimmunity. TNFR1 has been extensively studied and primarily mediates inflammation. TNFR2 remains far less studied, although emerging evidence demonstrates that TNFR2 plays an antiinflammatory and immunoregulatory role in various conditions and diseases. Herein, we report that TNFR2 regulates macrophage polarization, a highly dynamic process controlled by largely unidentified intracellular regulators. Using biochemical copurification and mass spectrometry approaches, we isolated the signaling molecule 14-3-3ε as a component of TNFR2 complexes in response to progranulin stimulation in macrophages. In addition, 14-3-3ε was essential for TNFR2 signaling–mediated regulation of macrophage polarization and switch. Both global and myeloid-specific deletion of 14-3-3ε resulted in exacerbated inflammatory arthritis and counteracted the protective effects of progranulin-mediated TNFR2 activation against inflammation and autoimmunity. TNFR2/14-3-3ε signaled through PI3K/Akt/mTOR to restrict NF-κB activation while simultaneously stimulating C/EBPβ activation, thereby instructing macrophage plasticity. Collectively, this study identifies 14-3-3ε as a previously unrecognized vital component of the TNFR2 receptor complex and provides new insights into the TNFR2 signaling, particularly its role in macrophage polarization with therapeutic implications for various inflammatory and autoimmune diseases with activation of the TNFR2/14-3-3ε antiinflammatory pathway.

Introduction

Rheumatoid arthritis (RA) is a common chronic autoimmune condition characterized by inflammatory joint disease (1), resulting from protracted inflammation of the synovial membrane. Macrophages are a major subset of the infiltrating immune cells present in the inflamed joint (2) and are central to the pathophysiology of inflammatory arthritis (3, 4). Functional plasticity is a hallmark of macrophages, and phenotypic polarization can occur at any point in the inflammatory process. Disparate phenotypic macrophages play critical but opposing roles in infectious and autoimmune diseases, inflammatory-associated cancers, and chronic metabolic diseases (5–7). Importantly, macrophage polarization is a highly dynamic process and the phenotype of polarized macrophages can switch under physiological and pathological conditions (8). Although the extracellular signals that induce macrophage phenotypic polarization have been well characterized (9), the intracellular regulators responsible for modulating macrophage polarization and switch are less well known.

TNF-α is a proinflammatory cytokine that is central to the inflammatory cascade in the pathogenesis of RA (10–12). There are 2 functionally distinct receptors of TNF-α: TNFR1 and TNFR2. TNFR1 primarily mediates inflammatory activity of TNF-α, whereas TNFR2 plays a protective and antiinflammatory role in various diseases and conditions (13–18). Evidence of divergent biologic roles for TNFR1 and TNFR2 in inflammatory arthritis was first reported by Blüml et al. (19), who demonstrated that TNFR1 and TNFR2 deficiencies have distinct and opposing phenotypes in a model of erosive arthritis, indicating an antiinflammatory role of TNFR2. Although TNFR2 signaling was reported to be involved in the function of macrophages (20, 21), TNFR2 signaling is far less well understood relative to TNFR1. In particular, the role of TNFR2 in macrophage plasticity remains unknown.

Progranulin (PGRN) was discovered as a ligand of TNFR2 in our genetic screen and exhibited an approximately 600-fold higher binding affinity to TNFR2 than TNF-α (22). Additionally, loss of PGRN rendered B6 mice highly susceptible to collagen-induced arthritis (CIA), whereas administration of recombinant PGRN prevented the onset and progression of inflammatory arthritis in both TNF-α transgenic and CIA models (22–24). Numerous independent laboratories, including ours, have implicated the importance of PGRN/TNFR2 interaction in various kinds of diseases (22, 25–34), including inflammatory arthritis.

Conflict of interest: The authors have declared that no conflict of interest exists.

Submitted: September 4, 2020; **Accepted:** June 25, 2021; **Published:** August 16, 2021.
Reference information: *J Clin Invest*. 2021;131(16):e144016.
https://doi.org/10.1172/JCI144016.

In the current study, we take advantage of PGRN's high TNFR2 binding feature to use it as a TNFR2 agonist to activate and delineate TNFR2 signaling. Using biochemical copurification and mass spectrometry approaches, we isolate the signaling molecule 14-3-3ε as a novel component of TNFR2 complexes in response to PGRN stimulation in macrophages. 14-3-3ε constitutes one of the vital signal molecules recruited by TNFR2, and the TNFR2/14-3-3ε complex supports an antiinflammatory phenotype in macrophages in inflammatory arthritis. In sum, our work uncovers the molecular mechanisms whereby TNFR2 signaling controls macrophage polarization and demonstrates the potential of targeting this pathway for the treatment of inflammatory and autoimmune disease.

Results

TNFR2 modulates macrophage polarization and switch. To determine whether and how antiinflammatory and immunoregulatory TNFR2 participated in regulation of macrophage polarization, we first determined the effect of TNFR2 deficiency on bone marrow–derived macrophages (BMDMs) polarized to M1 and M2 macrophages with LPS/IFN-γ and IL-4, respectively (Figure 1A). As shown in Figure 1B, TNFR2 deletion markedly enhanced the expression of the M1-specific marker genes *Il6* and *Nos2* upon LPS/IFN-γ stimulation. In contrast, TNFR2 deletion significantly suppressed the M2-specific marker genes *Arg1* and *Mgl1* upon IL-4 stimulation (Figure 1C). Given that macrophage polarization is a dynamic process and macrophages can switch their phenotype as tissue inflammation progresses, we examined whether TNFR2 also regulated the macrophage phenotypic switch in vitro (35, 36). More specifically, BMDMs isolated from WT and TNFR2$^{-/-}$ mice were polarized to M1 or M2 macrophages before inducing a phenotypic switch to M2 or M1 macrophages, respectively. Results demonstrated that TNFR2 deletion significantly enhanced the propensity of M2 macrophages to switch into an M1 phenotype but suppressed the phenotypic switch from M1 to M2 (Figure 1, D and E). In addition, flow cytometry analysis of BMDMs under the polarization conditions revealed a significant enhancement of M1 polarization and reduced M2 polarization in TNFR2$^{-/-}$ BMDMs as compared with WT BMDMs (Figure 1, F and G and Supplemental Figure 1; supplemental material available online with this article; https://doi.org/10.1172/JCI144016DS1). Furthermore, PGRN enhanced M2 and inhibited M1 polarization in WT BMDMs, but these effects were blunted in TNFR2$^{-/-}$ BMDMs (Figure 1, F and G). It was also noted that PGRN deficiency resulted in phenocopy of TNFR2 deficiency–associated alterations in macrophage polarization and phenotypic switch (Supplemental Figure 2).

We also compared the effects on macrophage polarization and phenotypic switch by activation of TNFR2 with 2 different TNFR2 activators: PGRN, known to activate TNFR2 in multiple cell types (22, 25–27, 37), and TY010, a specific TNFR2 agonist antibody (38). As expected, both PGRN and TY010 dramatically suppressed M1 polarization (Figure 1B) and promoted M2 polarization of WT macrophages to a similar extent (Figure 1C). Moreover, each activator significantly promoted an M1 to M2 switch and inhibited an M2 to M1 switch in WT macrophages. Notably, these effects on macrophage polarization and phenotypic switch were essentially abolished in macrophages with TNFR2 deletion. In addition, TNFR2 knockdown using siRNA in Raw264.7 macrophages could recapitulate the effects of TNFR2 deficiency in BMDMs in terms of modulating macrophage polarization and switch (Supplemental Figure 3, A–F).

In addition, TNF neutralizing antibody was used to determine whether PGRN's anti–TNF-α/TNFR1 activity contributed to its regulation on M2 polarization. Blockade of TNF activity with anti-TNF antibody did not affect PGRN-promoted M2 macrophage polarization (Supplemental Figure 4). Collectively, these results indicated that TNFR2 signaling was crucial for supporting an antiinflammatory phenotype in macrophages.

14-3-3ε is a component of the TNFR2 complex and required for TNFR2 signaling regulation of macrophage polarization. The finding that the TNFR2 signaling pathway played a pivotal role in controlling macrophage polarization and phenotypic switch led us to hypothesize that activation of TNFR2 by its agonists may recruit different cofactor(s) or adaptors to the receptor complexes, followed by activation of distinct intracellular signaling pathways and downstream gene expression. To isolate such cofactor(s), the intracellular domain (ICD) of TNFR2 was cloned into the PGEX-3X vector to express a fusion of GST to TNFR2ICD. As illustrated in Figure 2A, GST (serving as a control) or GST-TNFR2ICD was affinity purified on glutathione-agarose beads and used as a bait to trap proteins from PGRN-treated Raw264.7 macrophages. These samples were then analyzed by mass spectrometry and MS/MS spectra were searched against the Uniprot database, using Sequest within Proteome Discoverer. After subtracting the hits that were also trapped by the GST column, we found 7 proteins specifically bound to TNFR2 (Figure 2A). Identification of TRAF1 and TRAF2, 2 known TNFR-binding proteins, among the 7 hits validated the technique. The highest ranking protein was 14-3-3ε, a regulatory protein belonging to the 14-3-3 family that bound to a wide array of cellular proteins (39, 40). Accumulating evidence suggested that 14-3-3 proteins functioned as "adaptor" or "scaffold" proteins for the assembly of multiprotein signaling complexes (41–44). Thus, 14-3-3ε represented an attractive potential intracellular signaling mediator in the TNFR2 signaling pathway regulating macrophage polarization.

To characterize the role of 14-3-3ε in macrophage polarization, we generated myeloid cell–specific 14-3-3ε–deficient mice (Figure 2B) (hereafter referred to as 14-3-3ε^{LysM}) by crossing 14-3-3ε$^{fl/fl}$ mice (45) with LysM-Cre mice (46). 14-3-3ε^{LysM} mice were born in a Mendelian ratio and displayed no overt phenotype. Genomic DNA prepared from tail, T cells, hepatocytes, and macrophages were analyzed by PCR (Supplemental Figure 5). Knockout allele was only detectable in the macrophage DNA (Supplemental Figure 5C), indicating the Cre recombinase was efficient and specific for macrophages.

LysM-Cre initiated gene deletion within early hematopoietic progenitor cells, concomitant with its activity in neutrophils, which led us to consider whether myeloid-specific 14-3-3ε deficiency influenced macrophage and neutrophil differentiation and proliferation. We first analyzed bone morrow myeloid progenitor subpopulations, including common myeloid progenitors (CMPs), bipotential granulocyte/macrophage progenitors (GMPs), and megakaryocyte/erythrocyte progenitors (MEPs) in 14-3-3ε^{LysM} mice versus controls. 14-3-3ε deficiency neither exhibited apparent effects on CMPs, GMPs, and MEPs (Supplemental Figure 6, A–C), nor perturbed subsequent monocyte/macrophage and neutrophil maturation, as evidenced by indistinguishable frequency of CD11b$^+$F4/80$^+$ and CD11b$^+$Ly6G$^+$ cells in peripheral blood, spleen, and bone marrow

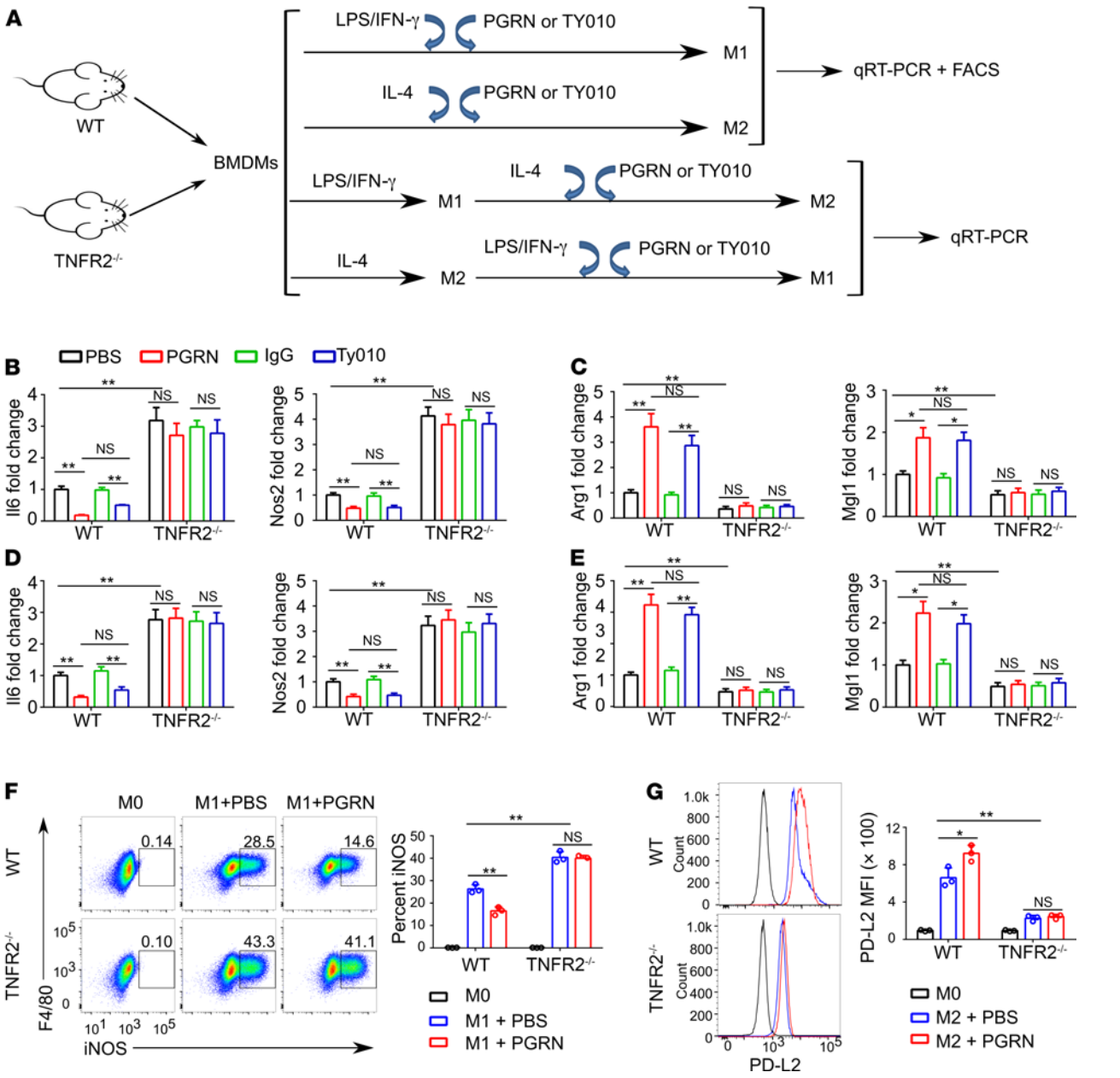

Figure 1. TNFR2 signaling controls macrophage polarization. (**A**) Schematic diagram illustrating the in vitro experimental design. (**B**) Fold change of *Il6* and *Nos2* mRNA in WT and TNFR2$^{-/-}$ BMDMs polarized to M1 with LPS/IFN-γ in the presence or absence of 0.5 μg/mL PGRN or 2.5 μg/mL TY010 for 18 hours. (**C**) Fold change of *Arg1* and *Mgl1* mRNA in WT and TNFR2$^{-/-}$ BMDMs polarized to M2 with IL-4 in the presence or absence of 0.5 μg/mL PGRN or 2.5 μg/mL TY010 for 18 hours. (**D** and **E**) BMDMs from WT and TNFR2$^{-/-}$ were polarized to M2 (IL-4) or M1 (LPS/IFN-γ) for 18 hours. Media were removed and M2 macrophages were treated with M1 stimuli (LPS/IFN-γ) while M1 macrophages were treated with M2 stimuli (IL-4) with or without 0.5 μg/mL PGRN or 2.5 μg/mL TY010 for an additional 18 hours. Quantitative PCR (qPCR) was performed to measure the expression of *Nos2* and *Il6*in M2 macrophages polarized to M1 (**D**), and the expression of *Arg1* and *Mgl1*in M1 macrophages polarized to M2 (**E**). (**F** and **G**) Flow cytometry analysis of WT and TNFR2$^{-/-}$ BMDMs polarized to M1 (**F**) or M2 (**G**) in the absence and presence of PGRN. CD45^{+}CD11b^{+} cells were gated, and iNOS^{+} cells or PD-L2 mean fluorescence intensity (MFI) were analyzed. Data are mean ± SD; n = 3 biological replicates; significant difference was analyzed by 1-way ANOVA with Bonferroni's post hoc test; $^{*}P < 0.05$ or $^{**}P < 0.01$.

(Supplemental Figure 7, A–C) from that of littermate controls. In addition, loss of 14-3-3ε in myeloid lineage did not affect the proliferation of bone marrow–derived macrophages and neutrophils in vitro (Supplemental Figure 7, D and E).

We also generated 14-3-3ε knockout Raw264.7 macrophages using CRISPR-Cas9 technique (Supplemental Figure 8, A and B). Coimmunoprecipitation with the lysate from control and 14-3-3ε knockout Raw264.7 macrophages, or 14-3-3ε$^{fl/fl}$ and 14-3-3ε^{LysM} BMDMs, was performed to confirm the interaction between TNFR2 and 14-3-3ε. As shown in Figure 2C and Supplemental Figure 8C, TNFR2 was specifically detectable in the immunoprecipitated complex from control macrophages but not 14-3-3ε–deficient macrophages, indicating that 14-3-3ε was associated with TNFR2 in macrophages upon stimulation with PGRN. Additionally, immunofluorescence cell staining revealed that 14-3-3ε colocalized with TNFR2 in PGRN-treated Raw264.7 macrophages (Supplemental

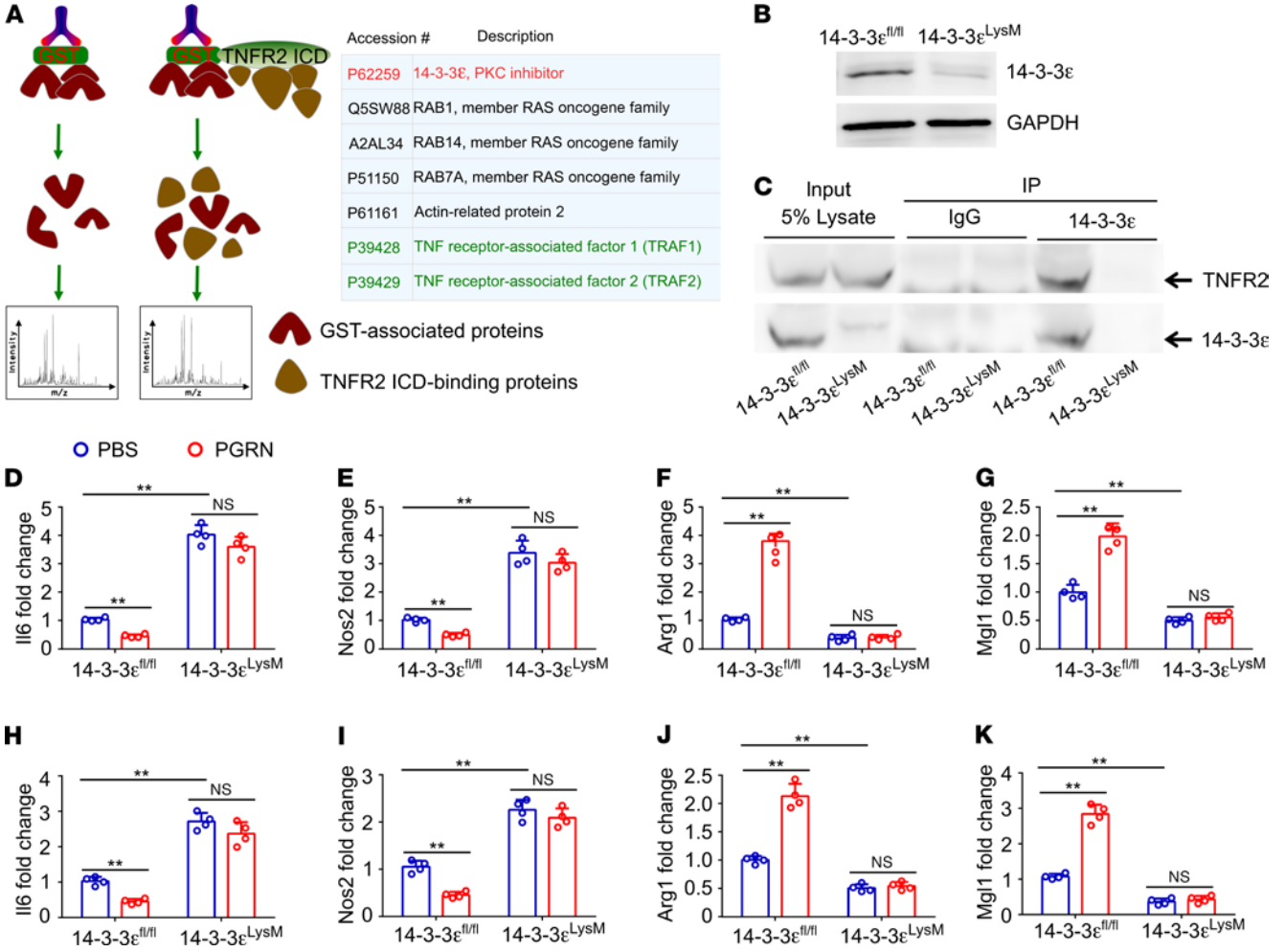

Figure 2. Activation of TNFR2 recruits 14-3-3ε during macrophage polarization. (**A**) Experimental design to identify potential molecules binding to TNFR2ICD upon PGRN stimulation. Summary of the hits that were specifically recruited to activated TNFR2 complexes in Raw264.7 macrophages. (**B**) Efficient ablation of 14-3-3ε in 14-3-3ε^{LysM} BMDMs, assayed by Western blotting. (**C**) Immunoprecipitation from 14-3-3ε$^{fl/fl}$ or 14-3-3ε^{LysM} BMDMs with 14-3-3ε antibody and detection of TNFR2 and 14-3-3ε by immunoblotting. Results shown are representative of 3 biological replicates. (**D**–**G**) 14-3-3ε$^{fl/fl}$ and 14-3-3ε^{LysM} BMDMs were polarized to M1 (LPS/IFN-γ) or M2 (IL-4) with or without 0.5 μg/mL PGRN for 18 hours, qPCR was performed to measure the expression of *Il6* (**D**), *Nos2* (**E**), *Arg1* (**F**), and *Mgl1* (**G**). (**H**–**K**) 14-3-3ε$^{fl/fl}$ and 14-3-3ε^{LysM} BMDMs were polarized to M2 (IL-4) or M1 (LPS/IFN-γ) for 18 hours, then M2 macrophages were treated with M1 stimuli (LPS/IFN-γ) while M1 macrophages were treated with M2 stimuli (IL-4) for an additional 18 hours. qPCR was performed to measure the expression of *Il6* (**H**) and *Nos2* (**I**) in M2 macrophages polarized to M1; expression of *Arg1* (**J**) and *Mgl1* (**K**) was measured in M1 macrophages polarized to M2. In **D**–**K**, data are mean ± SD; *n* = 4 biological replicates; significant difference was analyzed by 1-way ANOVA with Bonferroni's post hoc test; $^{**}P < 0.01$.

Figure 8D). Taken together, these results indicated that 14-3-3ε was recruited to activated TNFR2 receptor complex in macrophages.

To determine whether other 14-3-3 family members were also differentially regulated in M1 and M2 macrophages, and associated with PGRN or TNFR2, BMDMs isolated from WT, TNFR2$^{-/-}$, PGRN$^{-/-}$, and 14-3-3ε^{LysM} mice were polarized to M1 or M2. Successful polarization to M1 and M2 macrophages was confirmed by induction of M1 (*Il6*) and M2 (*Arg1*) specific gene expression, respectively (Supplemental Figure 9, A and B). Using primers specifically designed to detect all 7 isoforms of 14-3-3 family, we found that 14-3-3ε was the only isoform differentially regulated in M1 and M2 macrophages, its expression was downregulated in M1 and upregulated in M2 macrophages, and not affected by the deletion of either PGRN or TNFR2 (Supplemental Figure 9, C–I).

Next, we sought to determine whether 14-3-3ε was important for macrophage polarization and phenotypic switch, BMDMs isolated from 14-3-3ε$^{fl/fl}$ and 14-3-3ε^{LysM} mice were first polarized to M1 or M2 macrophages. Gene analysis showed that, as compared with 14-3-3ε$^{fl/fl}$ BMDMs, the genes typically linked to M1 macrophages, *Il6* and *Nos2*, were significantly upregulated in 14-3-3ε^{LysM} BMDMs, whereas *Arg1* and *Mgl1*, associated with the M2 macrophage phenotype, were markedly downregulated in 14-3-3ε^{LysM} BMDMs. Notably, the effects of TNFR2 activation on macrophage polarization and phenotypic switch were lost in 14-3-3ε^{LysM} BMDMs (Figure 2, D–K). In addition, similar results, in terms of enhanced M1 macrophages and M2 to M1 switch, and suppressed M2 macrophages and M1 to M2 switch, were also observed in 14-3-3ε knockout Raw264.7 cells (Supplemental Figure 10, A–D).

To further characterize the dependence of TNFR2 regulation of macrophage polarization on 14-3-3ε, flag-tagged 14-3-3ε was reexpressed in 14-3-3ε knockout Raw264.7 macrophages (Figure 3A). Reexpression of 14-3-3ε in 14-3-3ε knockout Raw264.7 macrophages

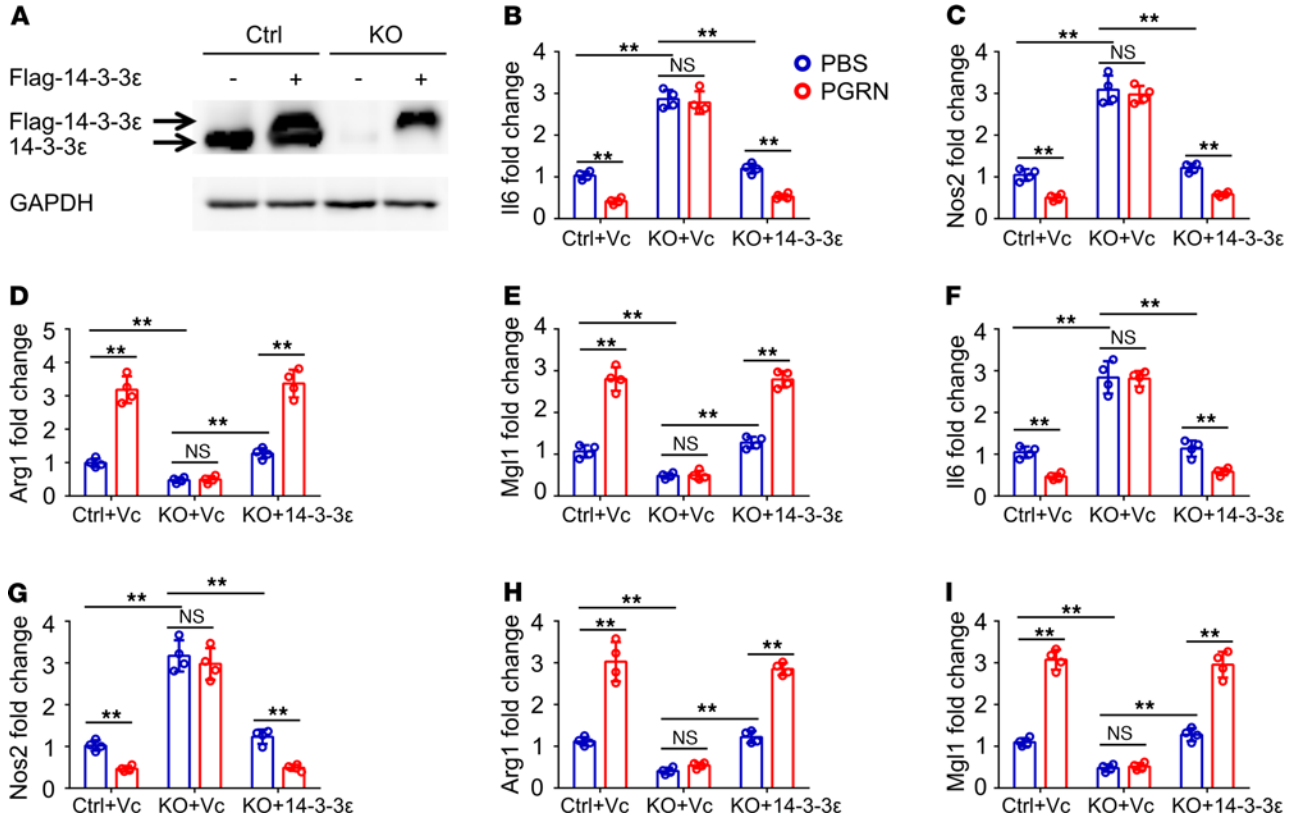

Figure 3. 14-3-3ε is required for TNFR2 signaling regulation of macrophage polarization. (**A**) Expression of Flag-14-3-3ε in 14-3-3ε$^{-/-}$ Raw264.7 cells. (**B**–**E**) Relative mRNA expression of *Il6* (**B**) and *Nos2* (**C**), or *Arg1* (**D**) and *Mgl1* (**E**) in control or 14-3-3ε$^{-/-}$ Raw264.7 cells with reexpression of 14-3-3ε, which were polarized to M1 or M2 with or without 0.5 μg/mL PGRN for 18 hours. (**F**–**I**) Expression of *Il6* (**F**) and *Nos2* (**G**), or *Arg1* (**H**) and *Mgl1* (**I**) in control or 14-3-3ε$^{-/-}$ Raw264.7 cells with reexpression of 14-3-3ε, which were polarized from M2 to M1 or M1 to M2 with or without 0.5 μg/mL PGRN for 18 hours, respectively. In **B**–**I**, data are mean ± SD; $n = 4$ biological replicates; significant difference was analyzed by 1-way ANOVA with Bonferroni's post hoc test; $^{**}P < 0.01$. Vc, empty vector; Flag-14-3-3ε, pCMV-Flag-14-3-3ε plasmid.

reversed the phenotype induced by 14-3-3ε deficiency. More importantly, reexpression could restore TNFR2 activation-mediated regulation of macrophage polarization and switch (Figure 3, B–I). In contrast, overexpression of 14-3-3ε in PGRN knockout Raw264.7 macrophages failed to reverse the effects of PGRN deficiency on macrophage regulation (Supplemental Figure 11, A–E). Collectively, these results indicated that 14-3-3ε was an essential mediator of TNFR2 signaling in controlling macrophage plasticity.

Loss of 14-3-3ε renders mice highly susceptible to collagen-induced arthritis and counteracts TNFR2 activation–mediated antiinflammation. To elucidate the in vivo role of TNFR2/14-3-3ε in general inflammation, we generated inducible 14-3-3ε global knockout mice (14-3-3ε$^{-/-}$) by breeding 14-3-3ε$^{fl/fl}$ mice with Rosa26a-CreERT2 mice in which Cre-mediated recombination was induced by tamoxifen (47), and then established collagen-induced arthritis (CIA), the most widely used inflammatory and autoimmune arthritis model, in 14-3-3ε$^{-/-}$ mice and control littermates. Deletion of 14-3-3ε resulted in more severe joint swelling and inflammation as evidenced by significantly higher clinical score, earlier disease onset and greater incidence of arthritis as compared with control mice (Figure 4A). Histological and quantitative analysis of whole ankle joints demonstrated 14-3-3ε deletion significantly increased synovitis, osteoclast activity, and destruction of bone and cartilage as compared with controls (Figure 4, B and C and Supplemental Figure 12). In contrast, injection of TNFR2 agonist PGRN resulted in markedly decreased inflammation, delayed disease onset, reduced incidence of arthritis, and decreased bone and cartilage destruction in 14-3-3ε$^{fl/fl}$ mice with CIA (Figure 4, A–C). More importantly, PGRN's protective effects were mostly abolished in 14-3-3ε$^{-/-}$ mice with CIA (Figure 4, A–C).

Flow cytometry analyses of the immune cells (Supplemental Figure 13A) isolated from arthritic joints indicated that neither TNFR2 activation by PGRN nor 14-3-3ε ablation altered macrophage frequency and proliferation (Figure 4, D and E). However, 14-3-3ε deletion markedly increased mean fluorescence intensity (MFI) of iNos (Figure 4F), simultaneous with a decrease of CD206$^+$ (Figure 4G) cells in CD11b$^+$F4/80$^+$ cells, consistent with a strong shift toward M1 macrophages as compared with control. Notably, TNFR2 activation by PGRN significantly decreased MFI of iNos (Figure 4F), while CD206$^+$ (Figure 4G) cells increased, and these effects depended on 14-3-3ε, as evidenced by abrogated shift toward to M2 macrophages in PGRN-treated 14-3-3ε–deficient mice, and indistinguishable frequency of M1 or M2 macrophages between PBS- and PGRN-treated 14-3-3ε–deficient mice with CIA (Figure 4, F and G). The number of neutrophils in the joints was comparable between 14-3-3ε$^{fl/fl}$ and 14-3-3ε$^{-/-}$ mice with CIA; however, PGRN tended to reduce neutrophil populations in a 14-3-3ε–independent manner, although the phenomenon did not reach statistical significance (Figure 4H). Neither PGRN nor 14-3-3ε deficiency affected

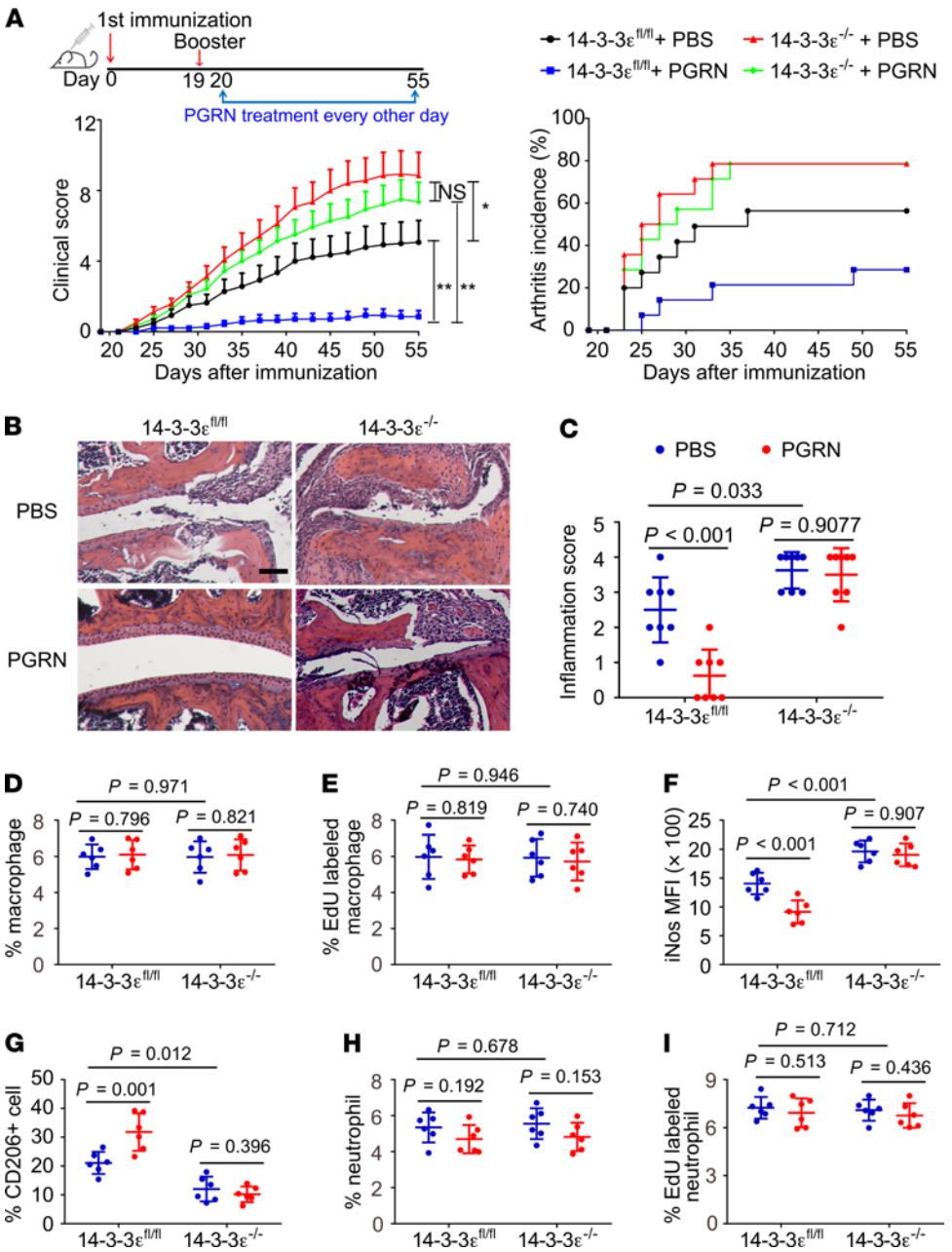

Figure 4. Global knockout of 14-3-3ε renders B6 mice highly susceptible to CIA. (**A**) Clinical arthritis scores and incidence of arthritis in the indicated mice with CIA. Data are mean ± SEM; $n = 14$ mice per group; significant difference was analyzed by 1-way ANOVA with Bonferroni's post hoc test; $^*P < 0.05$ or $^{**}P < 0.01$. (**B** and **C**) Representative images of H&E staining, and quantification of histomorphometric analysis of synovial inflammation of ankle joints ($n = 8$ mice per group). Scale bar: 100 μM. (**D**–**I**) The percentage of macrophages (**D**), Edu-labeled macrophages in total macrophages (**E**), iNOS mean fluorescence intensity (MFI) of macrophages (**F**), percentage of $CD206^+$ cells in $CD11b^+F4/80^+$ cells (**G**), percentage of neutrophils (**H**), and percentage of EdU-labeled neutrophils in total neutrophils (**I**) in the joints of indicated mice with CIA ($n = 6$ mice for each group) were determined by flow cytometry. In **C**–**I**, data are mean ± SD; significant difference was analyzed by 1-way ANOVA with Bonferroni's post hoc test.

neutrophil proliferation in arthritic joints (Figure 4I). Consistently, immunohistochemical staining for myeloperoxidase revealed that neutrophils present in inflamed joints were indistinguishable between 14-3-3$\varepsilon^{fl/fl}$ and 14-3-3$\varepsilon^{-/-}$ CIA mice and mice treated with PGRN exhibited mild reduction in activated neutrophils in the arthritic joints independent of 14-3-3ε (Supplemental Figure 14A).

In support of the notion that CIA induction led to systemic immune response in secondary lymphoid organs, including spleen, splenic macrophages displayed similar changes as those observed in arthritic joints. PGRN treatment and 14-3-3ε deletion did not affect the total number of macrophages in the spleen, whereas PGRN treatment increased M2 and inhibited M1 macrophages in a 14-3-3ε–dependent manner (Supplemental Figure 13C and Supplemental Figure 15, A–C). We previously reported that PGRN could also affect T cell subtypes in the course of inflammatory arthritis, so we determined whether these effects also depended on 14-3-3ε (Supplemental Figure 13, B and D). In line with our previous reports that regulation of Tregs contributed to PGRN/TNFR2's antiinflammation

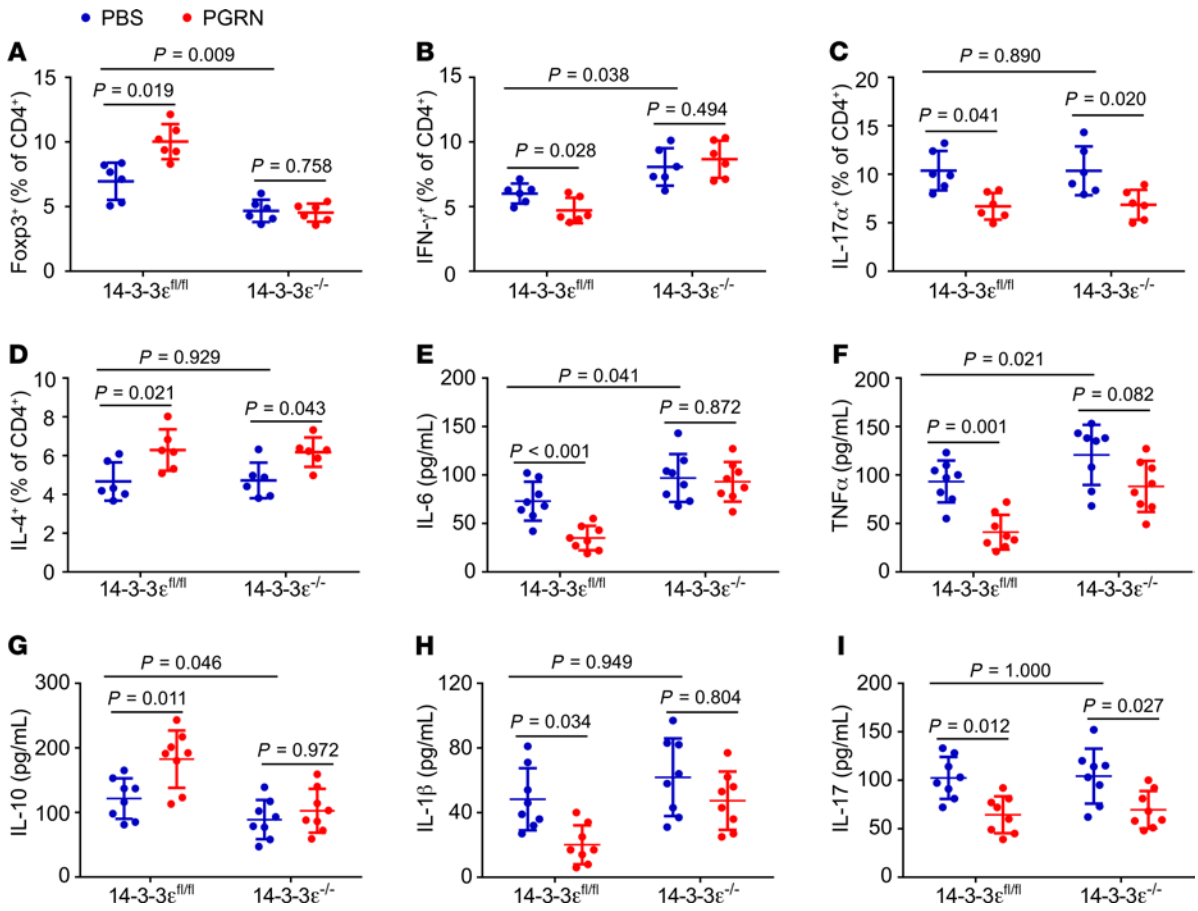

Figure 5. 14-3-3ε is implicated in mediating PGRN's regulation of T cells and inflammation in CIA. (**A**–**D**) Percentage of Treg (**A**), Th1 (**B**), Th17 (**C**), and Th2 (**D**) cells in CD4⁺ T cells in the joints of indicated mice with CIA (n = 6 for each group) were determined by flow cytometry. (**E**–**I**) Serum levels of IL-6 (**E**), TNF-α (**F**), IL-10 (**G**), IL-1β (**H**), and IL-17 (**I**) in the indicated mice with CIA (n = 8 mice for each group), assayed by ELISA. Data are mean ± SD; significant difference was analyzed by 1-way ANOVA with Bonferroni's post hoc test.

action (22, 26, 37), we found that 14-3-3ε deletion significantly reduced Treg cells in the joints and spleen compared with 14-3-3ε$^{fl/fl}$, whereas PGRN treatment markedly enhanced the Treg population compared with PBS treatment in 14-3-3ε$^{fl/fl}$ mice with CIA (Figure 5A and Supplemental Figure 15D). In addition, PGRN's regulation of Tregs was lost in 14-3-3ε$^{-/-}$ mice (Figure 5A and Supplemental Figure 15D). 14-3-3ε deficiency resulted in the increase of IFN-γ positive Th1 cells, while PGRN treatment led to reduction of this T cell population, PGRN regulation of Th1 cells was also abolished in 14-3-3ε$^{-/-}$ mice (Figure 5B and Supplemental Figure 15E). In contrast, 14-3-3ε deficiency did not affect Th2 and Th17 populations, and PGRN treatment significantly enhanced Th2 and reduced Th17 cells, respectively, in both 14-3-3ε$^{fl/fl}$ and 14-3-3ε$^{-/-}$ mice with CIA (Figure 5, C and D, Supplemental Figure 15, F and G), indicating that PGRN's regulation of Th2 and Th17 was 14-3-3ε independent.

We also examined the effects of 14-3-3ε deficiency on the serum levels of cytokines known to be involved in the pathogenesis of inflammatory and autoimmune arthritis. 14-3-3ε deletion boosted serum levels of proinflammation cytokines IL-6 and TNF-α while suppressed production of antiinflammation cytokine IL-10 as compared with 14-3-3ε$^{fl/fl}$ mice (Figure 5, E–G). In contrast, PGRN treatment significantly suppressed IL-6, TNF-α, and IL-1β (Figure 5, E, F, and H) and boosted IL-10 production (Figure 5G) in a 14-3-3ε–dependent manner. Interestingly, PGRN also suppressed the proinflammation cytokine IL-17, independent of 14-3-3ε (Figure 5I).

Similar results were observed in PGRN$^{-/-}$ CIA mice compared with WT counterparts. In this case, PGRN deletion also resulted in more severe inflammation, with predominance of proinflammatory M1 macrophages (Supplemental Figure 16, A–H and refs. 22, 26). In addition, PGRN deletion reduced percentages of Tregs, and increased percentages of Th1 and Th17 cells, but had no obvious effect on Th2 cells (Supplemental Figure 16, I–L).

Collectively, these results suggested that global 14-3-3ε deletion promoted an overt proinflammatory response in CIA, 14-3-3ε deletion could recapitulate the effects of PGRN deletion upon macrophage plasticity, and 14-3-3ε was an essential player in propagation of antiinflammatory PGRN/TNFR2 signaling in inflammatory and autoimmune arthritis.

Myeloid-specific deletion of 14-3-3ε exacerbates collagen-induced arthritis and abolishes PGRN/TNFR2 regulations of macrophages in vivo. To specifically address the role of myeloid-expressed 14-3-3ε in the etiology of inflammation and autoimmunity, and inflammatory and autoimmune arthritis in particular, we also established the CIA model in 14-3-3ε^{LysM} mice. First, we confirmed the efficient deletion of 14-3-3ε in macrophage present in the joints of 14-3-3ε^{LysM} mice with CIA (Supplemental Figure 17). Myeloid-specific 14-3-3ε deletion

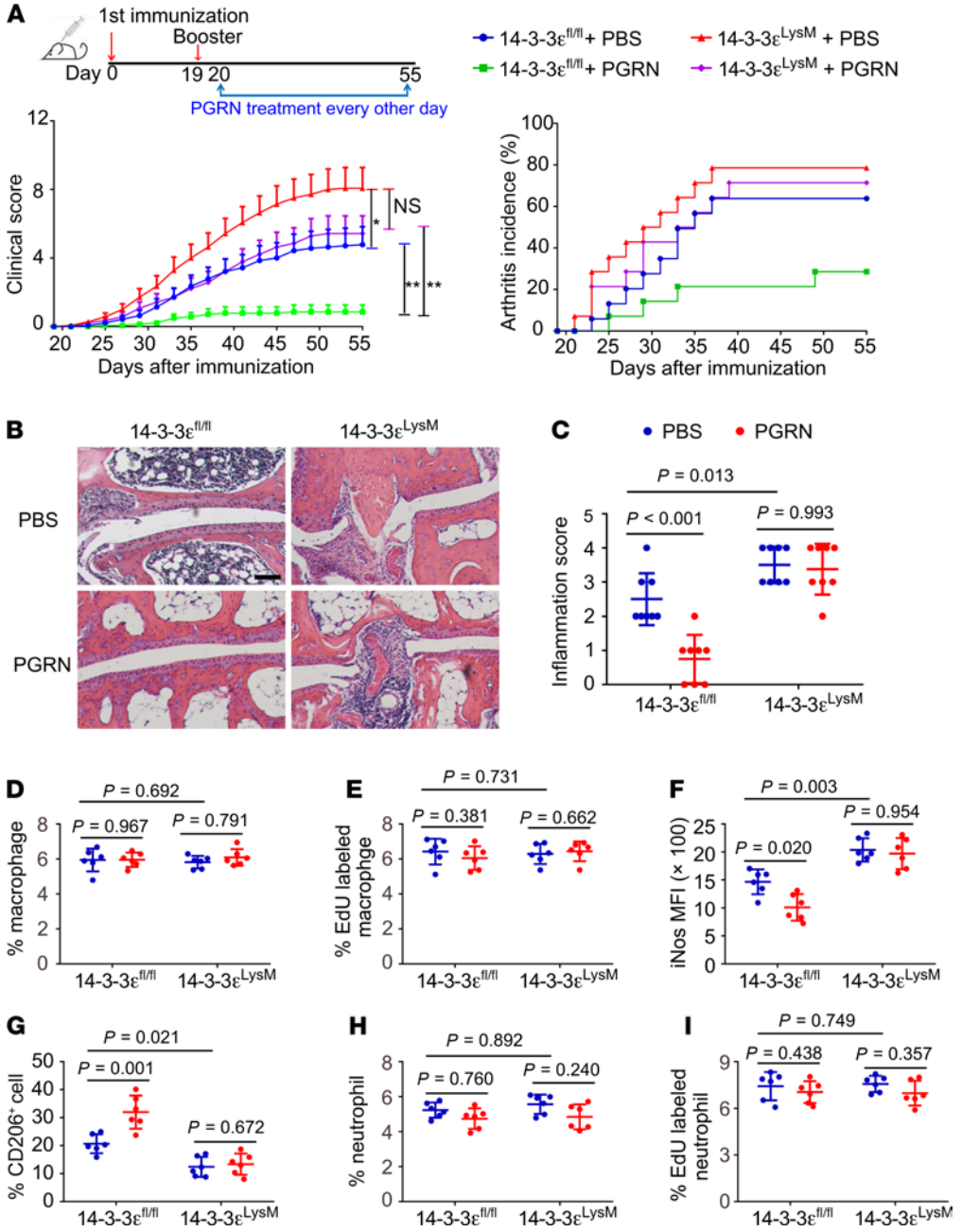

Figure 6. Myeloid-specific deletion of 14-3-3ε worsens inflammation in CIA. (**A**) Clinical arthritis scores and incidence of arthritis in the indicated mice with CIA. Data are mean ± SEM; $n = 14$ mice per group; significant difference was analyzed by 1-way ANOVA with Bonferroni's post hoc test; $^*P < 0.05$ or $^{**}P < 0.01$. (**B** and **C**) Representative images of H&E and quantification of histomorphometric analysis of synovial inflammation of ankle joints; $n = 8$ mice per group. Scale bar: 100 μM. (**D**–**I**) The percentage of macrophages (**D**), Edu-labeled macrophages in total macrophages (**E**), iNOS MFI of macrophages (**F**), percentage of CD206$^+$ cells in CD11b$^+$F4/80$^+$ cells (**G**), percentage neutrophils (**H**), and EdU-labeled neutrophils of total neutrophils (**I**) in the joints of indicated mice with CIA ($n = 6$ for each group) were determined by flow cytometry. In **C**–**I**, data are mean ± SD; significant difference was analyzed by 1-way ANOVA with Bonferroni's post hoc test.

resulted in more severe inflammation and earlier disease onset, and exacerbated bone and cartilage destruction relative to littermate 14-3-3ε$^{fl/fl}$ controls (Figure 6, A–C and Supplemental Figure 18). PGRN was administered to activate TNFR2 signaling in 14-3-3ε^{LysM} mice with CIA in order to determine the importance of myeloid 14-3-3ε for TNFR2 signaling regulation of inflammatory arthritis. PGRN treatment prompted mildly reduced inflammation relative to PBS treatment in 14-3-3ε^{LysM} mice with CIA, although differences did not reach statistical significance. Strikingly, PGRN's suppression of inflammation in 14-3-3ε^{LysM} mice was largely abolished relative to littermate 14-3-3ε$^{fl/fl}$ controls (Figure 6, A–C). In addition, 14-3-3ε^{LysM} mice had an increased number of osteoclasts relative to their littermate controls, whereas PGRN inhibited osteoclast number in a 14-3-3ε–dependent manner (Supplemental Figure 18, C and D). To investigate whether 14-3-3ε deficiency affected osteoclastogenesis in vitro, osteoclast differentiation was induced using BMDMs isolated from WT and 14-3-3ε^{LysM} mice. 14-3-3ε deficiency did not affect RANKL-induced osteoclastogenesis, but enhanced TNF-α and RANKL-costimulated

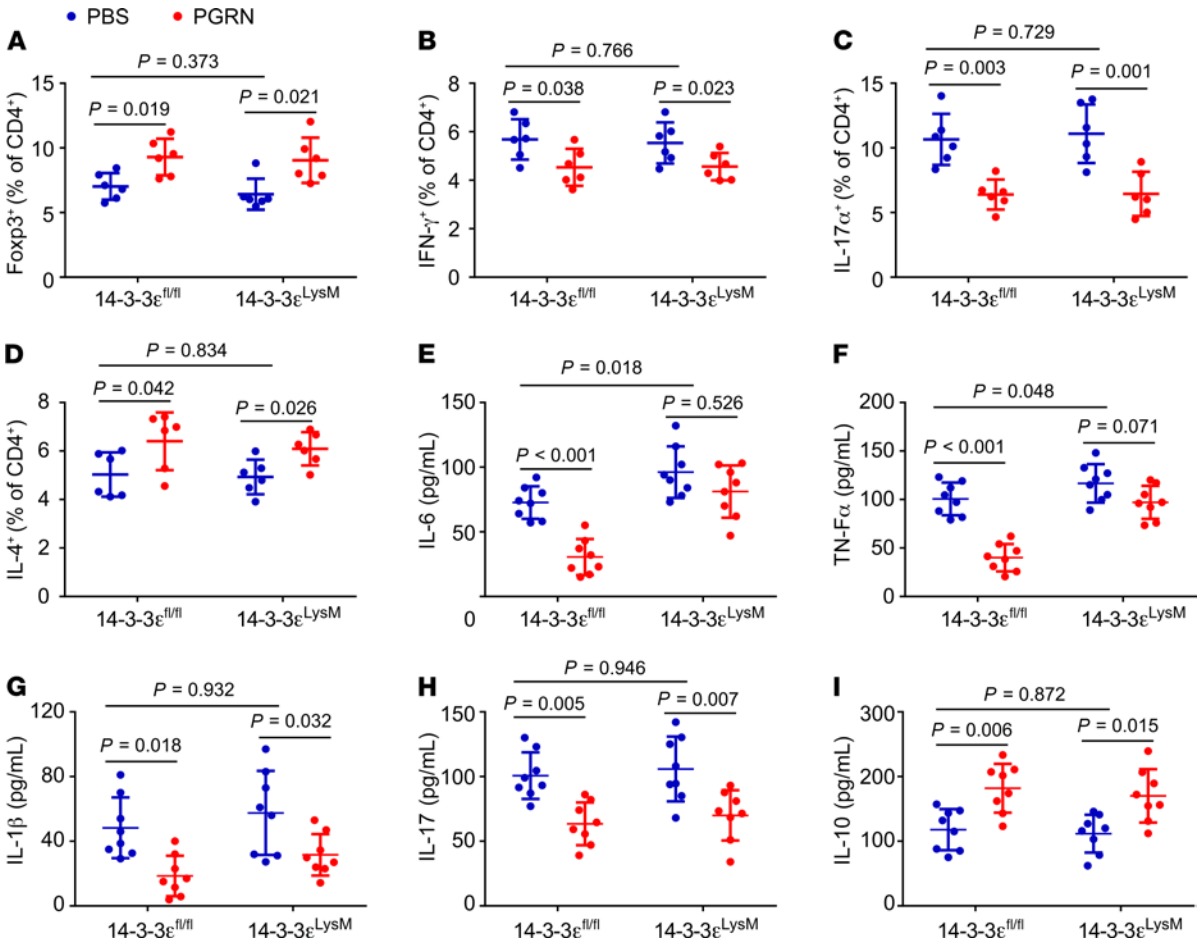

Figure 7. 14-3-3ε deficiency in myeloid lineage is implicated in PGRN regulation of serum levels in cytokines independent of T cells. (**A**–**D**) Percentage of Treg (**A**), Th1 (**B**), Th17 (**C**), and Th2 (**D**) cells in CD4+ T cells in the joints of indicated mice with CIA (n = 6 for each group) were determined by flow cytometry. (**E**–**I**) Serum levels of IL-6 (**E**), TNF-α (**F**), IL-1β (**G**), IL-17 (**H**), and IL-10 (**I**) in the indicated mice with CIA (n = 8 mice per group), assayed by ELISA. Data are mean ± SD; significant difference was analyzed by 1-way ANOVA with Bonferroni's post hoc test.

osteoclastogenesis. Additionally, PGRN inhibited TNF-α–enhanced osteoclastogenesis, which relied on 14-3-3ε (Supplemental Figure 19, A and B). These results suggested that increased osteoclasts seen in 14-3-3ε^{LysM} mice with CIA might also be attributed to disturbed osteoclastogenesis, apart from the elevated inflammation, which is known to promote osteoclastogenesis (48, 49).

Flow cytometry analysis revealed that total number and proliferation of macrophages infiltrated in inflamed joints were unchanged in 14-3-3ε^{LysM} mice relative to littermate 14-3-3ε$^{fl/fl}$ controls (Figure 6, D and E). Despite unchanged macrophage accumulation and proliferation in the arthritic joints, 14-3-3ε^{LysM} mice exhibited higher MFI of iNos, and lower CD206+ cells in CD11b$^+$F4/80$^+$ cells relative to littermate 14-3-3ε$^{fl/fl}$ controls (Figure 6, F and G), closely recapitulating the characteristic macrophage phenotype of 14-3-3ε$^{-/-}$ mice. Again, in a similar manner as seen in 14-3-3ε$^{-/-}$ mice, PGRN treatment skewed macrophages toward the M2 phenotype in 14-3-3ε$^{fl/fl}$ controls whereas this effect was lost in 14-3-3ε^{LysM} mice. Additionally, both recombinant PGRN and 14-3-3ε deficiency did not exert significant effects on number and proliferation of infiltrating neutrophils in the joints of the CIA mice (Figure 6, H and I and Supplementary 14B). As expected, myeloid-specific deletion of 14-3-3ε did not affect the T cell subtypes in the arthritic joints (Figure 7, A–D). Moreover, the phenotype of immune cells in spleen could closely recapitulate those in inflamed joints (Supplemental Figure 20, A–G). Analysis of serum cytokine levels demonstrated that IL-6 and TNF-α (Figure 7, E and F) were the major proinflammation cytokines impacted by myeloid-sourced 14-3-3ε given that all other cytokines measured (IL-1β, IL-17, and IL-10) were comparable between 14-3-3ε$^{fl/fl}$ and 14-3-3ε^{LysM} CIA mice (Figure 7, G–I). PGRN's regulation of IL-6 and TNF-α depended on macrophage 14-3-3ε, as evidenced by loss of these effects in 14-3-3ε^{LysM} CIA mice; however, PGRN's regulations of IL-1β, IL-17, and IL-10 production were independent of myeloid 14-3-3ε (Figure 7, E–I). Together, these results indicated that myeloid-expressed 14-3-3ε played an important role in TNFR2 signaling–mediated regulation of macrophages and anti-inflammatory activity in inflammatory and autoimmune arthritis.

14-3-3ε deficiency leads to the alterations of the intracellular signaling in macrophages. To elucidate the molecular mechanisms by which 14-3-3ε regulated macrophage plasticity, we performed unbiased RNA-seq on BMDMs isolated from 14-3-3ε$^{fl/fl}$ and 14-3-3ε^{LysM} mice stimulated with proinflammatory LPS/IFN-γ or antiinflammatory IL-4. Eight hundred fifteen genes (396 downregulated and 419 upregulated) were differentially expressed (fold change > 2, FDR < 0.05) in LPS-treated 14-3-3ε^{LysM} BMDMs compared with 14-3-3ε$^{fl/fl}$ BMDMs

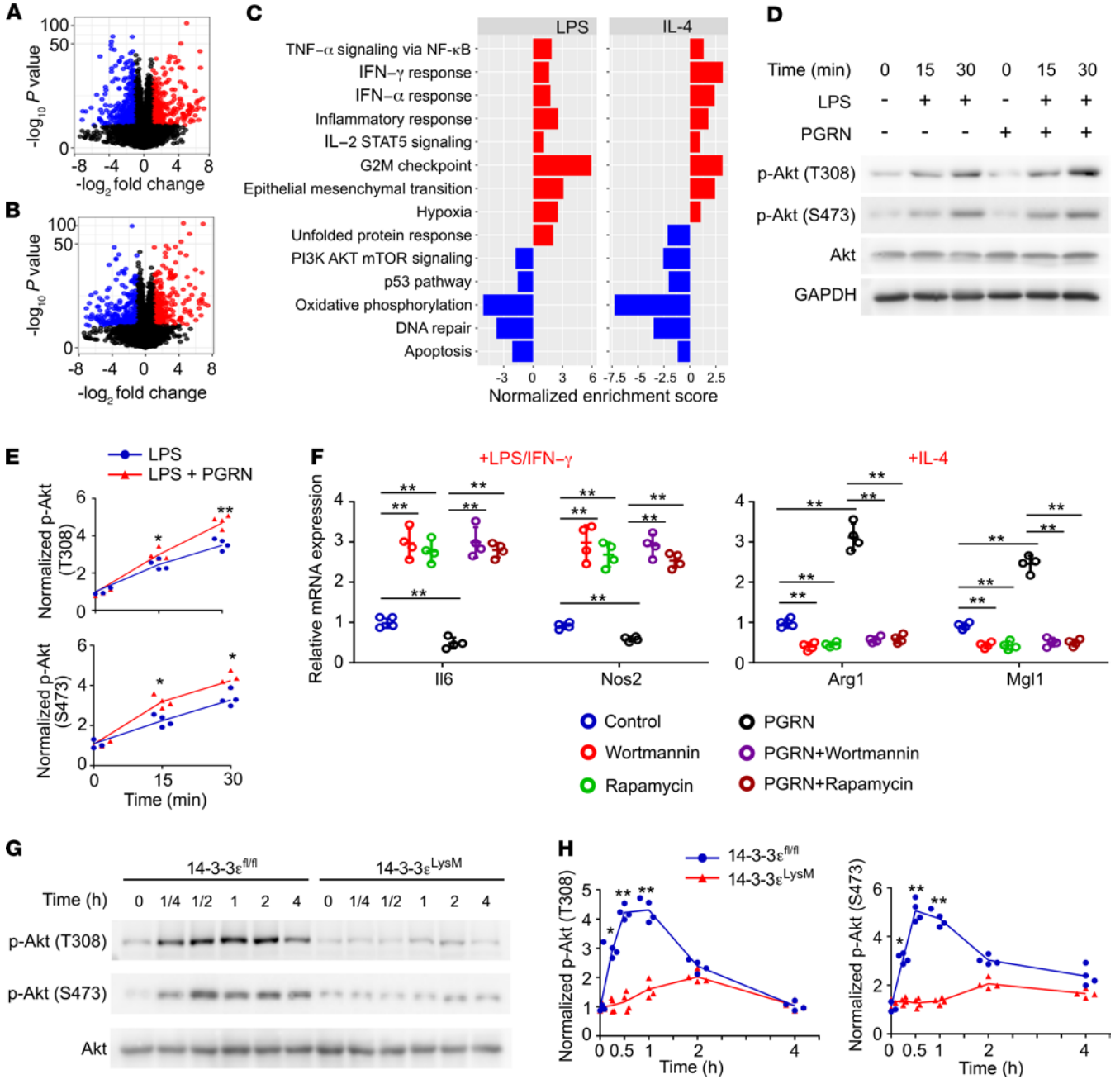

Figure 8. PI3K/Akt/mTOR pathway is involved in 14-3-3ε regulation of macrophage polarization. (**A** and **B**) Volcano plots of differentially expressed transcripts in LPS/IFN-γ (**A**) or IL-4 (**B**) polarized 14-3-3$\varepsilon^{fl/fl}$ and 14-3-3ε^{LysM} macrophages obtained by RNA sequencing; $n = 3$ biological replicates. Linear models with empirical Bayes statistic (Limma) were used for differential expression. Genes in red or blue are upregulated or downregulated, respectively, in 14-3-3ε^{LysM} as compared with 14-3-3$\varepsilon^{fl/fl}$ macrophage with Benjamini–Hochberg adjusted $P < 0.05$. (**C**) GSEA using hallmark gene sets from the Molecular Signature Database. The statistically significant signatures were filtered by gene sets with FDR less than 0.25. Red bars represented the pathways upregulated in the 14-3-3ε^{LysM} macrophages and blue bars indicated those enriched in 14-3-3$\varepsilon^{fl/fl}$ macrophages. (**D**) Immunoblotting of pAkt and Akt in LPS- and PGRN-stimulated WT BMDMs. GAPDH was used as the loading control. (**E**) Densitometry analysis of immunoblotting results shown in **D**. (**F**) mRNA expression in PI3K- or mTOR inhibitor–treated BMDMs polarized to M1 (LPS/IFN-γ) or M2 (IL-4) in the presence or absence of 0.5 μg/mL PGRN. (**G**) Immunoblotting of pAkt and Akt in 14-3-3$\varepsilon^{fl/fl}$ 14-3-3ε^{LysM} BMDMs stimulated with LPS. GAPDH was used as the loading control. (**H**) Densitometry analysis of immunoblotting results shown in **G**. In **D**–**H**, data are mean ± SD; n = 4 biological replicates; significant difference was analyzed by 1-way ANOVA with Bonferroni's post hoc test.

(Figure 8A and Supplemental Table 1), and 583 genes (291 downregulated and 292 upregulated) were differentially expressed (fold change>2, FDR<0.05) in IL-4–treated 14-3-3ε^{LysM} BMDMs compared with 14-3-3$\varepsilon^{fl/fl}$ BMDMs (Figure 8B and Supplemental Table 2). Similarly, PGRN deficiency was associated with an altered transcriptome pattern (Supplemental Figure 21, A and B). Gene set enrichment analysis (GSEA) revealed that both 14-3-3ε deficiency and PGRN deficiency altered gene expression patterns in macrophages. Specifically, genes associated with inflammation such as IFN-γ response, IFN -α response, and inflammatory response were largely upregulated

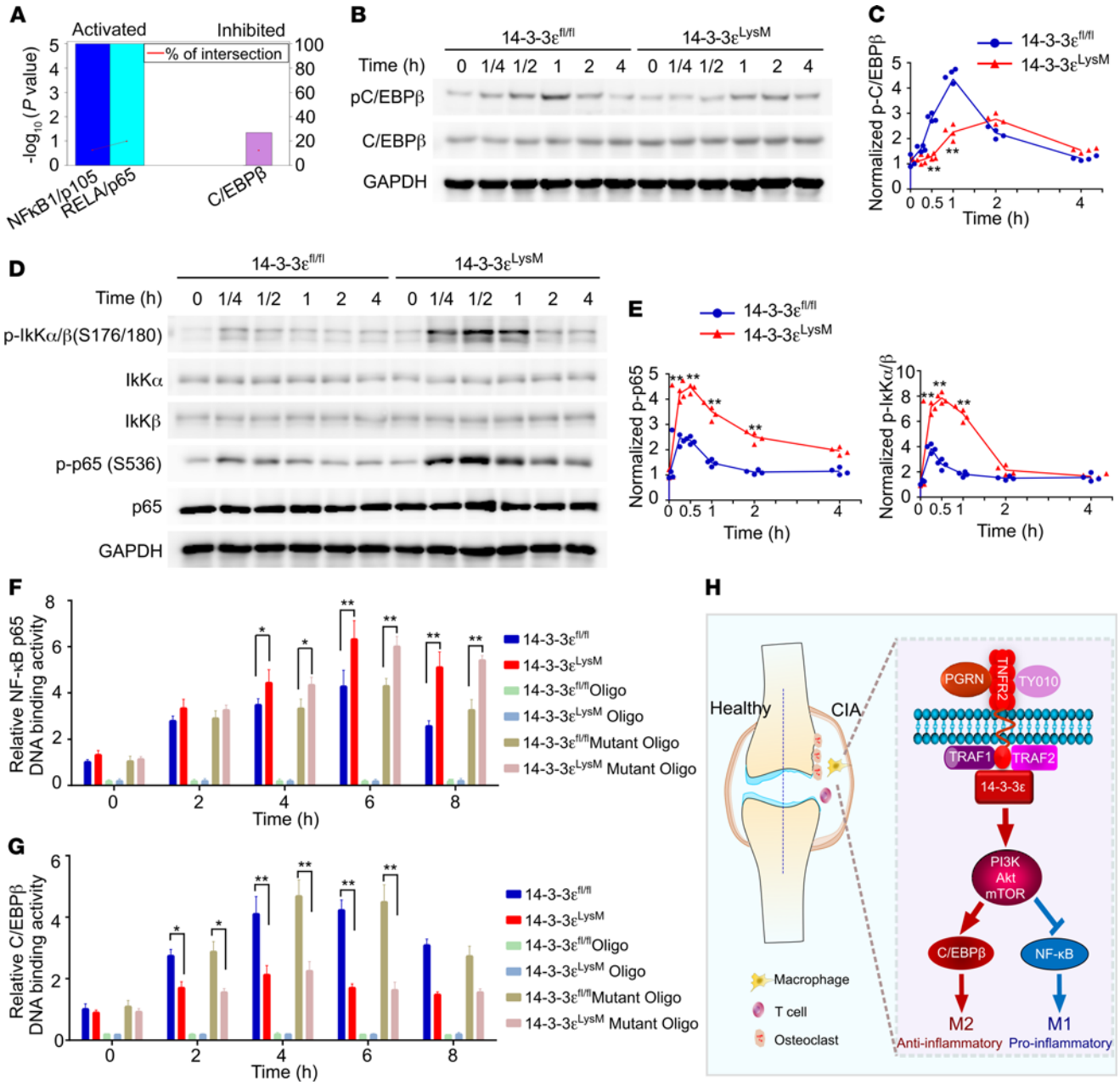

Figure 9. 14-3-3ε signals through NF-κB and C/EBPβ during macrophage polarization. (**A**) Transcription factors were predicted to be activated or inhibited and are implicated in the differential regulation of inflammation in 14-3-3ε^{LysM} compared with 14-3-3ε$^{fl/fl}$ BMDMs by TFactS analysis. (**B**) Immunoblot analysis of selected signaling molecules in IL-4–stimulated 14-3-3ε$^{fl/fl}$ and 14-3-3ε^{LysM} macrophages. (**C**) Densitometry analysis of immunoblotting results shown in **B**. (**D**) Immunoblot analysis of selected signaling molecules in LPS-stimulated 14-3-3ε$^{fl/fl}$ and 14-3-3ε^{LysM} macrophages. (**E**) Densitometry analysis of immunoblotting results shown in **D**. (**F**, **G**) NF-κB (**F**) and C/EBPβ (**G**) DNA binding activity in LPS- and IL-4–stimulated 14-3-3ε$^{fl/fl}$ and 14-3-3ε^{LysM} macrophages. For competitive binding studies, functional (oligo) or nonfunctional (mutant oligo) oligonucleotides were used according to the manufacturer's instructions. In **C**, **E**, **F**, and **G**, data are mean ± SD; $n = 4$ biological replicates; significant difference was analyzed by unpaired Student's t test (**C** and **E**) or 1-way ANOVA with Bonferroni's post hoc test (**F** and **G**); $^*P < 0.05$ or $^{**}P < 0.01$. (**H**) A proposed model depicting the signaling pathways by which PGRN/14-3-3ε/TNFR2 exerts antiinflammation effects through regulating macrophage polarization.

in 14-3-3ε^{LysM} and PGRN$^{-/-}$ BMDMs compared with WT BMDMs (Figure 8C, Supplemental Figure 21C, and Supplemental Figure 22, A–C). Intriguingly, GSEA analysis indicated that TNF-α/NF-κB and PI3K/Akt/mTOR signaling pathways were impaired in both 14-3-3ε–deficient and PGRN-deficient macrophages (Figure 8C, Supplemental Figure 21C, and Supplemental Figure 22, D and E) compared with WT BMDMs, suggesting that TNF-α signaling and PI3K signaling might be the key pathways regulated by the TNFR2/14-3-3ε complex in macrophage polarization. In addition, it was previously reported that PGRN activated Akt signaling and inhibited TNF-α signaling in various kinds of cells (50). Further, increasing evidence demonstrated that activation of the PI3K/Akt pathway was critical in restricting proinflammatory and promoting antiinflammatory response in macrophages (51–56). GSEA analysis, together with

these aforementioned reports, led us to examine whether PI3K/Akt/mTOR and TNF-α signaling were involved in the regulation of macrophage polarization by TNFR2/14-3-3ε. First, we examined the effect of PGRN on LPS-stimulated Akt phosphorylation and found that PGRN activated Akt phosphorylation in macrophages (Figure 8, D and E). In contrast, inhibition of PI3K or mTOR by their specific inhibitors was sufficient to enhance M1 macrophages and inhibit M2 macrophages, and block PGRN's effects on macrophage polarization (Figure 8F). Furthermore, both 14-3-3ε deficiency and PGRN deficiency inhibited LPS-stimulated Akt phosphorylation (Figure 8, G and H and Supplemental Figure 23A). In brief, PI3K/Akt/mTOR signaling was important for TNFR2/14-3-3ε signaling in regulating macrophage polarization.

TNFR2/14-3-3ε signaling inhibits NF-κB activation and stimulates C/EBPβ activation during macrophage polarization. GSEA analysis indicated that genes associated with inflammation, such as interferon response and inflammatory response, were largely upregulated in 14-3-3ε–deficient BMDMs compared with WT BMDMs. To further identify the transcription factor(s) that modulated enhanced inflammation in 14-3-3ε–deficient BMDMs, we searched for targets of these pathways using TFactS (57) and identified NF-κB1 (p105) and Rela (NF-κB p65) as significantly activated transcription factors and C/EBPβ as a significantly inhibited transcription factor in 14-3-3ε–deficient BMDMs (Figure 9A) that could modulate these inflammatory signaling pathways. The PI3K/Akt/mTOR signaling pathway was reported to act as a negative regulator of NF-κB signaling, leading to inhibited M1 macrophage response (54, 58, 59), but has also been linked to activation of transcription factor C/EBPβ, in turn promoting M2 macrophage response (54, 60). In line with the TFactS assay and previous reports, 14-3-3ε deficiency inhibited IL-4–stimulated C/EBPβ phosphorylation (Figure 9, B and C) and inhibited LPS-induced Akt phosphorylation while simultaneously enhanced LPS-induced phosphorylation of IκKα/β and NF-κB p65 (Figure 9D, E). Given that NF-κB p65 promoted the expression of proinflammatory cytokines (61, 62), whereas C/EBPβ promoted the expression of antiinflammatory cytokines in macrophages (60, 63, 64), we assessed the DNA binding activity of NF-κB p65 and C/EBPβ in macrophages in the presence or absence of 14-3-3ε. 14-3-3ε deficiency rapidly and sustainably enhanced LPS-stimulated p65 DNA binding activity as compared with WT macrophages (Figure 9F), whereas the opposite was seen for IL-4–induced C/EBPβ DNA binding activity (Figure 9G). These results indicated that 14-3-3ε acted as the suppressor of LPS/ NF-κB signaling in M1 macrophage polarization and the activator of IL-4/ C/EBPβ signaling in M2 macrophage polarization. In addition, PGRN deficiency also led to the inhibition of LPS-stimulated Akt phosphorylation and enhancement of LPS-stimulated phosphorylation of IκKα/β and NF-κB p65 (Supplemental Figure 23, A and B), whereas IL-4–stimulated C/EBPβ phosphorylation was inhibited (Supplemental Figure 23, C and D). Further, analogous to observations in 14-3-3ε–deficient macrophages, PGRN deficiency enhanced LPS-stimulated NF-κB p65 DNA binding (Supplemental Figure 23E) and suppressed IL-4–induced C/EBPβ DNA binding activity (Supplemental Figure 23F). Collectively, these mechanistic findings with 14-3-3ε–deficient and PGRN-deficient macrophages further implicated the importance of 14-3-3ε in PGRN/TNFR2 regulation of macrophage polarization.

Discussion

Inflammatory and autoimmune arthritis is a polyarticular chronic inflammatory disease characterized by deregulated immune response and bone erosion. Increasing evidence documents that macrophages significantly contribute to inflammation in inflammatory arthritis (5, 65), thus therapeutic strategies targeting the unbalanced M1/M2 ratio represent an attractive goal in treating inflammatory and autoimmune arthritis. Although it is well recognized that TNFR2 serves a beneficial antiinflammation function in inflammatory and autoimmune diseases, its role in macrophage polarization remains a poorly understood facet. Here, we found that TNFR2 played a critical role in regulating phenotypic polarization in macrophages. Activation of TNFR2 with its ligand PGRN markedly skewed the macrophage toward antiinflammatory M2 macrophages. Interestingly, in support of TNFR2 activation as a critical regulator of macrophage polarization, TY010, the specific TNFR2 agonist antibody (38), largely recapitulated the effects of PGRN on macrophage polarization. More importantly, using biochemical copurification and mass spectrometry approaches, we isolated the signaling molecule 14-3-3ε as a pivotal component of TNFR2 complexes in response to PGRN stimulation and a key participant of PGRN/TNFR2 signaling–mediated management of macrophage polarization, without affecting macrophage migration or proliferation.

14-3-3ε is a regulatory protein of the 14-3-3 family which binds to a wide array of cellular proteins (37, 38) and can function as adaptor or scaffold proteins for the assembly of multiprotein signaling complex (39–42).14-3-3ε deficiency in macrophages resulted in an overt proinflammatory response through skewing macrophages toward M1 phenotype in vitro. In addition, genetic 14-3-3ε deletion resulted in severe inflammation and unbalanced M1/M2 ratio relative to WT littermate controls, which suggested that unbalanced M1/M2 ratio played a pathologic role in inflammatory and autoimmune arthritis, and targeting macrophage plasticity through 14-3-3ε may hold therapeutic value. This study specifically focused on the role of intracellular 14-3-3ε, which was recruited to the TNFR2 intracellular domain following activation by TNFR2 ligand/agonist to mediate signaling through the TNFR2 pathway in macrophages. However, it has also been reported that extracellular 14-3-3ε could regulate chondrocyte metabolism (66). Whether and how extracellular 14-3-3ε regulates macrophage polarization, as well as functional comparisons of intracellular and extracellular 14-3-3ε in other cell types present in joints, including chondrocytes and osteocytes, warrants further investigation.

Several labs, including ours, have shown that the antiinflammatory activities of PGRN depended largely on TNFR2 (22, 25, 26, 31, 67). In current study, we successfully characterized 14-3-3ε as a component of TNFR2 complexes in macrophages. Our in vitro studies demonstrated that PGRN$^{-/-}$, TNFR2$^{-/-}$, and 14-3-3ε$^{-/-}$ macrophages exhibited enhanced M1 and reduced M2 polarization to comparable extent, while recombinant PGRN exerted opposite effects on macrophage polarization and these effects depended on TNFR2 and 14-3-3ε. Strikingly, the finding that reexpression of 14-3-3ε restored 14-3-3ε knockout cells' response to PGRN, while its overexpression failed to reverse PGRN deficiency's effects on macrophage polarization, indicated that 14-3-3ε served as an essential mediator of PGRN/TNFR2 signaling. Several findings, including enhanced susceptibility to murine CIA following global deletion of 14-3-3ε, recapitulation of global 14-3-3ε deletion's effects on macrophage

plasticity following myeloid-specific deletion of 14-3-3ε, and blockade of PGRN's antiinflammation action in 14-3-3ε–deficient CIA mice, provided genetic evidence demonstrating that 14-3-3ε was a crucial cofactor of TNFR2 and engaged in mediating TNFR2 signal's antiinflammatory phenotype. Furthermore, our data indicated IL-6 and TNF-α were 2 major proinflammatory cytokines secreted and regulated by macrophages via the TNFR2/14-3-3ε signaling pathway. The importance of IL-6 and TNF-α in mediating proinflammatory response and bone erosion had been highlighted by numerous experimental and clinical observations (4, 12, 68–70).

One limitation of using LysM-Cre to determine the role of PGRN/TNFR2/14-3-3ε in modulating macrophage plasticity during CIA was that LysM-Cre–mediated deletion of 14-3-3ε in neutrophils may also impact PGRN/TNFR2 regulation of inflammation in CIA. Neutrophil analyses with both 14-3-3$\varepsilon^{-/-}$ and 14-3-3ε^{LysM} revealed that 14-3-3ε deletion did not affect neutrophil infiltration in inflamed joints and PGRN's mild inhibition of neutrophils was independent of 14-3-3ε, indicating that the protection conferred by PGRN/TNFR2/14-3-3ε signaling in inflammatory arthritis was primarily attributable to their regulations of macrophage plasticity. Using a macrophage-specific Cre system such as Cx3cr1-Cre (71) can further confirm the importance of macrophage-expressed 14-3-3ε in mediating PGRN/TNFR2 signaling, which warrants further investigation. Although loss of 14-3-3ε did not alter total macrophages in the inflamed joints of mice with CIA, studies with a lineage tracing system (CCR2 or Cx3cr1) and subsequent characterization of the macrophages in the joints can be performed to further confirm the finding that 14-3-3ε signaling does not affect the total number of macrophages in the joints of mice with CIA, although it plays an important role in regulating macrophage plasticity.

In addition to its crucial role in mediating macrophage polarization, TNFR2/14-3-3ε signaling also regulated T cell subtypes associated with inflammatory and autoimmune arthritis, such as Tregs and Th1 cells. PGRN exhibited a broader range of effects on T cells in terms of inducing antiinflammatory Tregs and Th2 cells, while reducing proinflammatory Th17 and Th1 cells. Among these cell types, only the effects of PGRN on Tregs and Th1 depended on TNFR2/14-3-3ε, which might explain why PGRN's antiinflammatory effects were almost abolished in global 14-3-3ε knockout mice. PGRN's influence on T cell populations was significantly compromised in myeloid-specific 14-3-3ε knockout mice, but did not reach the same degree of obstruction observed in the global 14-3-3ε knockout mice. This difference emphasized the importance of employing cell-specific deletion of 14-3-3ε to assess the role of 14-3-3ε in individual cell subsets in the pathogenesis of inflammatory and autoimmune arthritis.

Our comparative transcriptome profiling and GSEA analysis of WT and 14-3-3ε or PGRN knockout macrophages demonstrated that both 14-3-3ε and PGRN deletion rendered macrophage populations constitutively more inflamed than WT controls, supporting the scenario that 14-3-3ε–dependent TNFR2 signaling plays an immunoregulatory and antiinflammatory role during inflammation. GSEA analysis also predicted that PI3K/Akt/mTOR and TNF signaling pathways may be engaged in TNFR2/14-3-3ε regulation of macrophage polarization. Subsequent inhibition of the PI3k signaling pathway using its inhibitors and examination of the activation status of key signaling molecules involved in these pathways, along with DNA binding activity analysis, revealed that TNFR2/14-3-3ε signaled through PI3K/Akt/mTOR to restrict NF-κB activation and simultaneously stimulate C/EBPβ activation, thereby instructing macrophage functional plasticity to promote immune suppression (Figure 9H).

In summary, our study identified 14-3-3ε as an important regulator of macrophage plasticity, which acted as a crucial cofactor of TNFR2 signaling. 14-3-3ε was necessary and sufficient to mediate TNFR2's regulation on macrophage polarization. The TNFR2/14-3-3ε pathway represented a mechanism by which macrophage balanced between proinflammatory and antiinflammatory responses and served as a promising candidate that could be targeted to regulate macrophage polarization. In addition, we provided proof of principle for the potential of exogenous PGRN to promote antiinflammation through regulating macrophage plasticity in the CIA model. These findings enable us to better understand the molecular mechanisms of TNFR2/14-3-3ε regulation of inflammation and autoimmunity, and more excitingly, may provide a rational for targeting the beneficial TNFR2 signaling pathway as a novel therapeutic approach for inflammatory arthritis and other inflammatory and autoimmune diseases in which macrophage polarization plays key pathogenic roles.

Methods

Mice. TNFR2$^{-/-}$, LysM-Cre, and Rosa26a-CreERT2 mice were obtained from The Jackson Laboratory. 14-3-3$\varepsilon^{fl/fl}$ mice were provided by Kazuhito Toyo-oka, and mated with transgenic mice expressing LysM-Cre and Rosa26a-CreERT2 to obtain myeloid and global 14-3-3ε knockout mice, respectively. For activation of CreERT2 in adult mice, 150 mg/kg body weight of tamoxifen (Sigma-Aldrich) in sunflower seed oil (Sigma-Aldrich) was intraperitoneally injected into 10-week-old mice once a day for 5 consecutive days. Littermate controls were used for all experiments. Genotyping for these mice was performed by PCR as previously reported (45). PGRN-deficient mice were established and maintained by the laboratory (22). All animals were housed on a 12-hour light-dark cycle with ad libitum access to food and water in a specific pathogen–free environment. Animals were maintained on a B6 background and were sex- and age-matched for experiments, typically between 10- and 12-weeks-of-age.

Preparation of rhPGRN. Generation of our recombinant PGRN stable cell line and purification of recombinant PGRN have been described in our previous publication (72). In brief, stable cells were cultured in DMEM that contained 1 mg/mL G418. PGRN was affinity purified from the medium of starved cells by using nickel nitrilotriacetic-agarose. The purity of recombinant PGRN was determined by SDS-PAGE.

CIA model. Ten-week-old mice were immunized via 0.1-mL intradermal injection of 100 mg chicken type II collagen (Chondrex) emulsified with an equal volume of complete Freund's adjuvant (CFA) that contained 4 mg/mL heat denatured *Mycobacterium* (Chondrex) at the base of the tail (d0), followed by a booster immunization with chicken type II collagen emulsified in incomplete Freund's adjuvant at day 19. In the CIA mouse model, clinical signs of arthritis in the paws were evaluated and scored individually by using a 0 to 4 point scoring system. Scores from each individual paw were summed to yield an overall score for each mouse, with a maximum score of 16 (73). Scores were attributed as follows: a paw score of 0, no signs; 1, mild swelling confined to the tarsal bones or ankle joint; 2, mild swelling extending from ankle to the tarsal bones; 3, moderate swelling extending from ankle to the metatarsal joints; and 4, severe swelling encompassing the ankle, foot, and digits and/or ankylosis of the limb. To determine therapeutic effects, recombinant PGRN (5 mg/kg body weight) was intraperitoneally injected into mice starting from

day 20 after first immunization on alternating days until euthanasia. Incidence was taken as equal to the ratio of CIA mice to the total number of mice exposed to the emulsion injections, multiplied by 100.

Histological analysis of mouse joints. Mouse joint tissues were fixed in 4% paraformaldehyde, decalcified in EDTA, and embedded in paraffin. Tissue sections were then prepared and stained with H&E. H&E-stained sections were scored for inflammation and bone erosion. Inflammation was scored according to the following criteria: (a) no inflammation, (b) slight thickening of the lining layer or some infiltrating cells in the underlying layer, (c) slight thickening of the lining layer plus some infiltrating cells in the underlying layer, (d) thickening of the lining layer, an influx of cells in the underlying layer, and presence of cells in the synovial space, and (e) synovium highly infiltrated with many inflammatory cells. Cartilage damage was determined by Safranin O staining, and the extent of cartilage damage was scored according to the following criteria: (a) no destruction, (b) minimal erosion limited to single spots, (c) slight-to-moderate erosion in a limited area, (d) more extensive erosion, and (e) general destruction (74). TRAP staining was used to determine bone erosion as previously described (22). The sections were imaged using a Zeiss microscope, and osteoclast quantification was performed using ImageJ software.

Immunohistochemistry staining. For immunohistochemistry staining, deparaffinized and hydrated sections were incubated with 0.1% trypsin for 30 minutes at 37°C, followed by 0.25 U/mL chondroitinase ABC (Sigma-Aldrich) and 1 U/mL hyaluronidase (Sigma-Aldrich) for 60 minutes at 37°C, respectively. Then the sections were incubated with antibodies against myeloperoxidase (1:100, PA5-16672, Invitrogen) overnight at 4°C. Detection was performed using the Vectastain Elite ABC kit (Vector) and positive signal was visualized with 0.5 mg/mL 3,3-diaminobenzidine in 50 mM Tris-Cl substrate (Sigma-Aldrich) and counterstained with 1% methyl green. Images were acquired with a Zeiss microscope.

Flow cytometry analysis. Single-cell suspensions from joint, spleen, or BMDMs were subjected to flow cytometry analysis. To prepare the single-cell suspensions from joints, the hind paws were harvested as previously described (75, 76). After the skins were removed, the paws were minced and digested in digestion buffer (2 mg/mL collagenase D, 2 mg/mL diapause II, and 1 mg/mL DNase I in HBSS) for 60 minutes at 37°C. Antibodies used were FITC-conjugated anti-CD4 (clone GK1.5), APC-conjugated anti-CD25 (clone PC61.5), eFluor 450-conjugated anti–IL-17 (clone eBio17B7), PE-conjugated anti–IL-4 (clone 11B11), APC-CY™7–conjugated IFN-γ (clone XMG1.2), biotin-conjugated anti-Foxp3 (clone FJK-16s), FITC-conjugated CD11b (clone M1/70), eFluor 450–conjugated anti-CD45 (clone 30-F11), APC-conjugated iNOS (clone CXNFT), PE-conjugated anti-CD206 (clone MMR), PE-cyanine5–conjugated anti-CD4 (clone RM4-5) (all from eBioscience); and streptavidin-conjugated Qdot 605 (Thermo Fisher Scientific). For myeloid progenitor experiments, bone marrow cells were stained with the following antibodies for lineage markers: CE3e (clone 145-2C11) PE-cyanine 7, B220 (clone RA3-6B2) PE-cyanine 7, CD14 (clone Sa14-2) PE-cyanine 7, CD4 (clone GK1.5) PE-cyanine 7, CD8 (clone 53-6.7) PE-cyanine 7, Ter119 (clone TER-119) PE-cyanine 7, Gr1 (clone RB6-8C5) PE-cyanine 7, CD16/32 (clone 93) APC, cKit (clone 2B8) APC-eFluor 780, Scal (clone D7) Pacific Blue, CD34 (clone RAM34) FITC and IL-7Rα (clone A7R34) PE-cyanine 5. Cells were acquired using a Becton Dickinson LSR Fortessa and analyzed by FlowJo and FCS Express.

Determining the proliferative capacity of cells. To assess cell proliferation in the joints of mice with CIA, EdU was injected into the mice at 50 mg/kg body weight twice per week for a week before the mice were sacrificed as previously described (77). After isolating cells from the joints, the Click-iT EdU kit from Invitrogen with Alexa Fluor 488 was used to detect the incorporated EdU as per the manufacturer's guidelines.

Determining LysM-Cre deletion efficiency in macrophages of the inflamed joints. Macrophages were purified from arthritic joins of 14-3-3$\varepsilon^{fl/fl}$ and 14-3-3ε^{LysM} CIA mice using MagniSort mouse F4/80 positive selection kit (Invitrogen). DNA extracted from the purified macrophages was used as template to detect the 14-3-3ε floxed allele and knockout band as previously reported (45).

Generation of 14-3-3ε knockout and PGRN knockout Raw264.7 by CRISPR-Cas9. Knockout cells were generated in accordance with a previously published protocol (78). Briefly, 14-3-3ε or PGRN sgRNA was inserted into the lentiCRISPR V2 vector (Addgene). Cotransfection of CRISPR plasmid, psPAX2, and pMD2.G (Addgene) into HEK293T (ATCC) was performed to produce the lentivirus. Then Raw264.7 (ATCC) were infected with the collected lentivirus for 18 hours, followed by selection with 2 μg/mL puromycin (Gibco) for 2 days.

Isolation of BMDMs and neutrophils and differentiation of BMDMs. Bone marrow cells were collected from the mice and cultured in α-MEM supplemented with 10% FBS and 10 ng/mL M-CSF (Biolegend) over 7 days for macrophage differentiation. Differentiated BMDMs were stimulated with 100 ng/mL LPS (Sigma-Aldrich) plus 20 ng/mL IFN-γ (Peprotech) or 20 ng/mL IL-4 (Peprotech) for 18 hours to polarize cells to M1 or M2 macrophages in the presence or absence of PGRN or TY010 (provided by Denise Faustman, Harvard Medical School, Boston, Massachusetts, USA), respectively. For inhibitor studies, PI3K inhibitor wortmannin (100 nM, Sigma-Aldrich) or mTOR inhibitor rapamycin (100 nM, Sigma-Aldrich) were incubated with macrophages for 1 hour before the addition of polarizing stimuli.

Bone marrow neutrophils were isolated by the negative selection technique using an EasySep Mouse Neutrophil Enrichment Kit (Stemcell Technologies).

Osteoclast differentiation and TRAP staining. BMDMs were obtained as described above and cultured with α-MEM supplemented with 10% FBS, 10 ng/mL M-CSF, 50 ng/mL RANKL (R&D), 20 ng/mL TNF-α, and 500 ng/mL PGRN for 5 days. The medium was replaced every day. TRAP staining was performed and the number of TRAP-positive multinucleated cells ($TRAP^+$-MNCs) containing more than 3 nuclei were counted using microscopy as described (22).

RNA-seq and bioinformatics analysis. Freshly isolated mouse bone marrow cells from 9 WT, 9 14-3-3ε^{LysM}, and 9 $PGRN^{-/-}$ mice were pooled into 3 replicate sets of WT, 14-3-3ε^{LysM}, and $PGRN^{-/-}$ cells and differentiated into macrophages for 7 days in α-MEM supplemented with 10%FBS and 10 ng/mL M-CSF. Each replicate set of macrophages was then treated with IL-4 or IFN-γ/LPS. Total RNA was extracted from BMDMs with RNeasy Mini Kit (Qiagen). mRNA was isolated from purified DNA-free RNA for library preparation. Libraries were sequenced on Illumina HiSeq 4000 by the NYU Genome Technology Center. Reads for genes were called using RSEM program (79) and differentially expressed genes were discovered using DESeq2 package (80). Significantly differentially expressed genes were defined by a 2-fold change with a false discovery ratio (FDR) less than or equal to 0.05. Genes that were significantly up- and downregulated in 14-3-3ε^{Lysm} compared with 14-3-3$\varepsilon^{fl/fl}$ BMDMs and were implicated in TNF-α and PI3K/Akt/mTOR pathways were used for transcription factor enrichment analysis with TFactS (57). All RNA-seq data sets used in this study have been deposited in the NCBI's Gene Expression Omnibus database (GEO GSE172119).

Individual quantitative RT–PCR. Total RNA was extracted from BMDMs with the RNeasy Mini Kit (Qiagen). cDNA was prepared using 1 μg RNA with the High-Capacity cDNA Reverse Transcription Kit (Applied Biosystems). SYBR green–based (Applied Biosystems) quantitative PCR was performed in triplicate using human and mouse primers to *Arg1*, *Mgl1*, *Il6*, *Nos2*, and *Gapdh* (Real-Time PCR System, Applied Biosystems). mRNA levels were normalized to *Gapdh* and reported as relative mRNA fold change.

Transcription factor DNA binding assays. NF-κB p65 and C/EBPβ DNA binding activity were measured by TransAM transcription factor assay kits (catalog 43296 and 44196, Active Motif). WT, 14-3-3ε^{LysM}, and PGRN$^{-/-}$ BMDMs were stimulated with 100 ng/mL LPS plus 20 ng/mL IFN-γ or 20 ng/mL for the indicated time, and nuclear extracts were prepared in lysis buffer AM2 (Active Motif). Nuclear extracts were incubated with the immobilized consensus sequence and p65 or C/EBPβ was detected using specific antibodies. For competitive binding studies, functional (oligo) or nonfunctional (mutant oligo) oligonucleotides were used according to the manufacturer's instructions.

Biochemical copurification and mass spectrometry. To isolate the cofactors of the PGRN/TNFR2 complex that mediate the intracellular signaling through TNFR2, the intracellular domain (ICD) of TNFR2 was cloned into the PGEX-3X vector to express a fusion of GST to TNFR2ICD. GST (serving as a control) or GST-TNFR2ICD was affinity-purified on glutathione-agarose beads and used as a bait to trap proteins from RAW264.7 cells treated with 500 ng/mL PGRN for 30 minutes. These samples were then analyzed by mass spectrometry, performed by NYU Proteomics Laboratory. All MS/MS spectra were collected using the following instrument parameters: resolution of 15,000, AGC target of 1×10^5, maximum ion time of 120 ms, 1 microscan, 2 m/z isolation window, fixed first mass of 150 m/z, and NCE of 27. MS/MS spectra were searched against a Uniprot Human database using Sequest within Proteome Discoverer 1.4.

Immunoprecipitation. BMDMs isolated from 14-3-3ε$^{fl/fl}$ and 14-3-3ε^{LysM} mice or control and 14-3-3ε knockout Raw264.7 macrophages were treated with PGRN for 30 minutes prior to lysis in RIPA buffer containing protease inhibitors. Total protein (400 μg) was immunoprecipitated with anti-14-3-3ε antibody, the protein complexes were detected with anti-TNFR2 and 14-3-3ε antibodies.

Immunoblotting. IL-4– and LPS-treated macrophage cultures were solubilized in RIPA buffer containing protease and phosphatase inhibitors. Total protein (50 μg) was separated by SDS-PAGE and electroblotted onto nitrocellulose membranes (Bio-Rad Laboratories) using a wet transfer system. Proteins were detected by incubation with 1:1000 dilutions of primary antibodies, washed and incubated with appropriate secondary antibodies, and detected after incubation with a chemiluminescent substrate. Primary antibodies against Akt (catalog 9272), p-AKT Thr308 (catalog 4056), p-Akt Ser473 (catalog 4058), IκKα (catalog 2682), IκKβ (catalog 8943), p-IκKα/β (catalog 2697), p65 (catalog 4764), p-p65 (catalog 3033), C/EBPβ (catalog 3087), p-CEBPβ (catalog 3084) were purchased from Cell Signaling Technology, and 14-3-3ε (catalog sc-393177), PGRN (catalog sc-28928), and TNFR2 (catalog sc-7862) antibodies were purchased from Santa Cruz Biotechnology.

ELISA assay. Levels of IL-6, IL-1β, TNF-α, IL-17, and IL-10 were detected in sera isolated from murine models using ELISA kits in accordance with the manufacturer's instructions (Invitrogen).

Statistics. The numbers of mice used per genotype are indicated in figure legends. Comparisons between 2 groups were analyzed using 2-tailed unpaired Student's *t* tests. The 1-way ANOVA with Bonferroni's post hoc test was used when comparing multiple groups. A value of P less than 0.05 was considered statistically significant.

Study approval. All animal studies were performed in accordance with institutional guidelines and approved by the IACUC of New York University School of Medicine.

Author contributions

WF and CJL designed the experiments and wrote the manuscript. WF executed most experiments. W Hu performed RNA-seq analysis and assisted with flow cytometry analysis. YSY assisted with protein immunoprecipitation. AH, GS, YB, W He, LZ, GG, and JL assisted with protein purification and animal experiments. KT provided 14-3-3ε$^{fl/fl}$ mice. DBS, GX, and PL participated in analyzing the data and editing the manuscript.

Acknowledgments

This work was supported in part by NIH research grants R01AR062207, R01AR061484, R01AR076900, R01NS103931, and R01NS096098 and Department of Defense research grant W81XWH-16-1-0482. We would like to acknowledge all lab members for insightful discussions. We greatly appreciate Denise Faustman at Harvard Medical School for providing the TNFR2 agonist TY010. We also thank the NYU Genome Technology Center and Proteomics Laboratory for technical support.

Address correspondence to: Chuan-ju Liu, Department of Orthopedic Surgery, NYU Grossman School of Medicine, 301 East 17th Street, New York, New York 10003, USA. Email: chuanju.liu@nyulangone.org.

1. Scott DL, et al. Rheumatoid arthritis. *Lancet*. 2010;376(9746):1094–1108.
2. Kinne RW, et al. Cells of the synovium in rheumatoid arthritis. Macrophages. *Arthritis Res Ther*. 2007;9(6):224.
3. Udalova IA, et al. Macrophage heterogeneity in the context of rheumatoid arthritis. *Nat Rev Rheumatol*. 2016;12(8):472–485.
4. Siouti E, Andreakos E. The many facets of macrophages in rheumatoid arthritis. *Biochem Pharmacol*. 2019;165:152–169.
5. Funes SC, et al. Implications of macrophage polarization in autoimmunity. *Immunology*. 2018;154(2):186–195.
6. Tabas I, Glass CK. Anti-inflammatory therapy in chronic disease: challenges and opportunities. *Science*. 2013;339(6116):166–172.
7. Wynn TA, et al. Macrophage biology in development, homeostasis and disease. *Nature*. 2013;496(7446):445–455.
8. Wang N, et al. Molecular mechanisms that influence the macrophage m1-m2 polarization balance. *Front Immunol*. 2014;5:614.
9. Mantovani A, et al. The chemokine system in diverse forms of macrophage activation and polarization. *Trends Immunol*. 2004;25(12):677–686.
10. Sedger LM, McDermott MF. TNF and TNF-receptors: from mediators of cell death and inflammation to therapeutic giants - past, present and future. *Cytokine Growth Factor Rev*. 2014;25(4):453–472.
11. Williams A, et al. Review: novel insights into tumor necrosis factor receptor, death receptor 3, and progranulin pathways in arthritis and bone remodeling. *Arthritis Rheumatol*. 2016;68(12):2845–2856.
12. Keffer J, et al. Transgenic mice expressing human tumour necrosis factor: a predictive genetic model of arthritis. *EMBO J*. 1991;10(13):4025–4031.
13. Bluml S, et al. Targeting TNF receptors in rheumatoid arthritis. *Int Immunol*. 2012;24(5):275–281.
14. Peschon JJ, et al. TNF receptor-deficient mice reveal divergent roles for p55 and p75 in several models of inflammation. *J Immunol*. 1998;160(2):943–952.

15. Cui Y, et al. Progranulin: a conductor of receptors orchestra, a chaperone of lysosomal enzymes and a therapeutic target for multiple diseases. *Cytokine Growth Factor Rev*. 2019;45:53–64.
16. Tseng WY, et al. TNF receptor 2 signaling prevents DNA methylation at the *Foxp3* promoter and prevents pathogenic conversion of regulatory T cells. *Proc Natl Acad Sci U S A*. 2019;116(43):21666–21672.
17. Monaco C, et al. Anti-TNF therapy: past, present and future. *Int Immunol*. 2015;27(1):55–62.
18. Muller J, et al. Tumor necrosis factor receptor superfamily in T cell priming and effector function. *Adv Immunol*. 2018;140:21–57.
19. Bluml S, et al. Antiinflammatory effects of tumor necrosis factor on hematopoietic cells in a murine model of erosive arthritis. *Arthritis Rheum*. 2010;62(6):1608–1619.
20. Ruspi G, et al. TNFR2 increases the sensitivity of ligand-induced activation of the p38 MAPK and NF-κB pathways and signals TRAF2 protein degradation in macrophages. *Cell Signal*. 2014;26(4):683–690.
21. Sheng Y, et al. TNF receptor 2 makes tumor necrosis factor a friend of tumors. *Front Immunol*. 2018;9:1170.
22. Tang W, et al. The growth factor progranulin binds to TNF receptors and is therapeutic against inflammatory arthritis in mice. *Science*. 2011;332(6028):478–484.
23. Liu CJ. Progranulin: a promising therapeutic target for rheumatoid arthritis. *FEBS Lett*. 2011;585(23):3675–3680.
24. Liu CJ, Bosch X. Progranulin: a growth factor, a novel TNFR ligand and a drug target. *Pharmacol Ther*. 2012;133(1):124–132.
25. Wei F, et al. PGRN protects against colitis progression in mice in an IL-10 and TNFR2 dependent manner. *Sci Rep*. 2014;4:7023.
26. Fu W, et al. Foxo4- and Stat3-dependent IL-10 production by progranulin in regulatory T cells restrains inflammatory arthritis. *FASEB J*. 2017;31(4):1354–1367.
27. Zhao YP, et al. Progranulin protects against osteoarthritis through interacting with TNF-α and β-Catenin signalling. *Ann Rheum Dis*. 2015;74(12):2244–2253.
28. Zhang K, et al. Elevated progranulin contributes to synaptic and learning deficit due to loss of fragile X mental retardation protein. *Brain*. 2017;140(12):3215–3232.
29. Huang K, et al. Progranulin is preferentially expressed in patients with psoriasis vulgaris and protects mice from psoriasis-like skin inflammation. *Immunology*. 2015;145(2):279–287.
30. Vezina A, et al. Mesenchymal stromal cell ciliogenesis is abrogated in response to tumor necrosis factor-α and requires NF-κB signaling. *Cancer Lett*. 2014;345(1):100–105.
31. Zhou M, et al. Progranulin protects against renal ischemia/reperfusion injury in mice. *Kidney Int*. 2015;87(5):918–929.
32. Li H, et al. Circulating PGRN is significantly associated with systemic insulin sensitivity and autophagic activity in metabolic syndrome. *Endocrinology*. 2014;155(9):3493–3507.
33. Yang D, et al. Progranulin promotes colorectal cancer proliferation and angiogenesis through TNFR2/Akt and ERK signaling pathways. *Am J Cancer Res*. 2015;5(10):3085–3097.
34. Liu J, et al. PGRN induces impaired insulin sensitivity and defective autophagy in hepatic insulin resistance. *Mol Endocrinol*. 2015;29(4):528–541.
35. Kadl A, et al. Identification of a novel macrophage phenotype that develops in response to atherogenic phospholipids via Nrf2. *Circ Res*. 2010;107(6):737–746.
36. Adamson SE, et al. Disabled homolog 2 controls macrophage phenotypic polarization and adipose tissue inflammation. *J Clin Invest*. 2016;126(4):1311–1322.
37. Wei F, et al. Progranulin facilitates conversion and function of regulatory T cells under inflammatory conditions. *PLoS One*. 2014;9(11):e112110.
38. Okubo Y, et al. Homogeneous expansion of human T-regulatory cells via tumor necrosis factor receptor 2. *Sci Rep*. 2013;3:3153.
39. Aitken A, et al. 14-3-3 proteins: biological function and domain structure. *Biochem Soc Trans*. 1995;23(3):605–611.
40. Fu H, et al. 14-3-3 proteins: structure, function, and regulation. *Annu Rev Pharmacol Toxicol*. 2000;40:617–647.
41. Barry EF, et al. 14-3-3:Shc scaffolds integrate phosphoserine and phosphotyrosine signaling to regulate phosphatidylinositol 3-kinase activation and cell survival. *J Biol Chem*. 2009;284(18):12080–12090.
42. Dougherty MK, Morrison DK. Unlocking the code of 14-3-3. *J Cell Sci*. 2004;117(pt 10):1875–1884.
43. Aitken A. 14-3-3 proteins: a historic overview. *Semin Cancer Biol*. 2006;16(3):162–172.
44. Mackintosh C. Dynamic interactions between 14-3-3 proteins and phosphoproteins regulate diverse cellular processes. *Biochem J*. 2004;381(pt 2):329–342.
45. Toyo-oka K, et al. 14-3-3ε and ζ regulate neurogenesis and differentiation of neuronal progenitor cells in the developing brain. *J Neurosci*. 2014;34(36):12168–12181.
46. Clausen BE, et al. Conditional gene targeting in macrophages and granulocytes using LysMcre mice. *Transgenic Res*. 1999;8(4):265–277.
47. Ventura A, et al. Restoration of p53 function leads to tumour regression in vivo. *Nature*. 2007;445(7128):661–665.
48. Wei S, et al. IL-1 mediates TNF-induced osteoclastogenesis. *J Clin Invest*. 2005;115(2):282–290.
49. Wu L, et al. Tumor necrosis factor alpha promotes osteoclast formation Via PI3K/Akt pathway-mediated blimp1 expression upregulation. *J Cell Biochem*. 2017;118(6):1308–1315.
50. Chitramuthu BP, et al. Progranulin: a new avenue towards the understanding and treatment of neurodegenerative disease. *Brain*. 2017;140(12):3081–3104.
51. Covarrubias AJ, et al. Control of macrophage metabolism and activation by mTOR and Akt signaling. *Semin Immunol*. 2015;27(4):286–296.
52. Fukao T, Koyasu S. PI3K and negative regulation of TLR signaling. *Trends Immunol*. 2003;24(7):358–363.
53. Troutman TD, et al. Toll-like receptors, signaling adapters and regulation of the pro-inflammatory response by PI3K. *Cell Cycle*. 2012;11(19):3559–3567.
54. Kaneda MM, et al. PI3Kgamma is a molecular switch that controls immune suppression. *Nature*. 2016;539(7629):437–442.
55. Katholnig K, et al. Immune responses of macrophages and dendritic cells regulated by mTOR signalling. *Biochem Soc Trans*. 2013;41(4):927–933.
56. Wang S, et al. Metabolic reprogramming of macrophages during infections and cancer. *Cancer Lett*. 2019;452:14–22.
57. Essaghir A, et al. Transcription factor regulation can be accurately predicted from the presence of target gene signatures in microarray gene expression data. *Nucleic Acids Res*. 2010;38(11):e120.
58. Weichhart T, Saemann MD. The multiple facets of mTOR in immunity. *Trends Immunol*. 2009;30(5):218–226.
59. Luyendyk JP, et al. Genetic analysis of the role of the PI3K-Akt pathway in lipopolysaccharide-induced cytokine and tissue factor gene expression in monocytes/macrophages. *J Immunol*. 2008;180(6):4218–4226.
60. Sahin E, et al. Macrophage PTEN regulates expression and secretion of arginase I modulating innate and adaptive immune responses. *J Immunol*. 2014;193(4):1717–1727.
61. Ben-Neriah Y, Karin M. Inflammation meets cancer, with NF-κB as the matchmaker. *Nat Immunol*. 2011;12(8):715–723.
62. Bonizzi G, Karin M. The two NF-kappaB activation pathways and their role in innate and adaptive immunity. *Trends Immunol*. 2004;25(6):280–288.
63. Gray MJ, et al. Induction of arginase I transcription by IL-4 requires a composite DNA response element for STAT6 and C/EBPbeta. *Gene*. 2005;353(1):98–106.
64. El Kasmi KC, et al. Toll-like receptor-induced arginase 1 in macrophages thwarts effective immunity against intracellular pathogens. *Nat Immunol*. 2008;9(12):1399–406.
65. Tardito S, et al. Macrophage M1/M2 polarization and rheumatoid arthritis: a systematic review. *Autoimmun Rev*. 2019;18(11):102397.
66. Priam S, et al. Identification of soluble 14-3-3 as a novel subchondral bone mediator involved in cartilage degradation in osteoarthritis. *Arthritis Rheum*. 2013;65(7):1831–1842.
67. Yan W, et al. Progranulin controls sepsis via C/EBPα-regulated Il10 transcription and ubiquitin ligase/proteasome-mediated protein degradation. *J Immunol*. 2016;197(8):3393–3405.
68. Williams RO, et al. Anti-tumor necrosis factor ameliorates joint disease in murine collagen-induced arthritis. *Proc Natl Acad Sci U S A*. 1992;89(20):9784–9788.
69. Ohshima S, et al. Interleukin 6 plays a key role in the development of antigen-induced arthritis. *Proc Natl Acad Sci U S A*. 1998;95(14):8222–8226.
70. Boe A, et al. Interleukin 6 knock-out mice are resistant to antigen-induced experimental arthritis. *Cytokine*. 1999;11(12):1057–1064.
71. Yona S, et al. Fate mapping reveals origins and dynamics of monocytes and tissue macrophages under homeostasis. *Immunity*. 2013;38(1):79–91.
72. Feng JQ, et al. Granulin epithelin precursor: a bone morphogenic protein 2-inducible growth factor that activates Erk1/2 signaling and JunB transcription factor in chondrogenesis. *FASEB J*. 2010;24(6):1879–1892.

73. Brand DD, et al. Collagen-induced arthritis. *Nat Protoc*. 2007;2(5):1269–1275.
74. Camps M, et al. Blockade of PI3Kgamma suppresses joint inflammation and damage in mouse models of rheumatoid arthritis. *Nat Med*. 2005;11(9):936–943.
75. Li J, et al. BAD inactivation exacerbates rheumatoid arthritis pathology by promoting survival of sublining macrophages. *Elife*. 2020;9:e56309.
76. Misharin AV, et al. Nonclassical Ly6C(-) monocytes drive the development of inflammatory arthritis in mice. *Cell Rep*. 2014;9(2):591–604.
77. Murphy MP, et al. Articular cartilage regeneration by activated skeletal stem cells. *Nat Med*. 2020;26(10):1583–1592.
78. Ran FA, et al. Genome engineering using the CRISPR-Cas9 system. *Nat Protoc*. 2013;8(11):2281–2308.
79. Li B, Dewey CN. RSEM: accurate transcript quantification from RNA-Seq data with or without a reference genome. *BMC Bioinformatics*. 2011;12:323.
80. Love MI, et al. Moderated estimation of fold change and dispersion for RNA-seq data with DESeq2. *Genome Biol*. 2014;15(12):550.